https://doi.org/10.5194/egusphere-2026-3250
Preprint. Discussion started: 30 July 2026

Opposite-sign influences of canopy structural and physiological dynamics on water–carbon biogeography

Daniel Short Gianotti[1] and Dara Entekhabi[1]

[1]Parsons Laboratory for Environmental Science and Engineering, Department of Civil and Environmental Engineering, Massachusetts Institute of Technology, Cambridge, USA

Correspondence: Daniel Short Gianotti (gianotti@mit.edu)

Abstract. The terrestrial water and carbon cycles are strongly coupled through both vegetation canopy extent (structural) dynamics and canopy-intensive, physiological water-use dynamics. Although landscape vegetation productivity is directly proportional to both canopy extent and water use efficiency by definition, they are negatively correlated with each other at monthly scale, and their roles in connecting carbon uptake with water variables are in opposition. This study separates the roles of structural and physiological dynamics in driving a functional biogeographical pattern. We show that the relationship between Gross Primary Production (GPP) and Evaporative Fraction (EF, the normalized ratio of evaporation to available energy) more strongly links local temporal behavior with spatial biogeographical patterns than do rain-use efficiency relationships. This GPP–EF relationship has opposite correlation at daily ($n = 325,374$) and monthly timescales ($n = 11,776$): daily dynamics evolve toward a monthly "attractor" curve, while monthly correlations are positive and align with an across-site, across-biome, biogeographical relationship. Similarly, vegetation canopy extent and EF show the same timescale-dependent pattern: canopy extent increases with daily drying (negative correlation), then co-evolves positively with EF at monthly scales. The relationship between EF and physiological, canopy-averaged water-use efficiency is negatively-correlated at all scales. At monthly and longer timescales, structural canopy dynamics dominate water–carbon coupling over physiological water-use responses.

These results imply that modeling water–carbon feedbacks at timescales beyond daily requires accurate representation of both (a) dynamic canopy extent and (b) canopy-averaged water-use efficiency, or risk conflating opposite-sign correlations with changes in productivity. Specifically, vegetation growth, mortality, and responsive canopy phenology (structural processes) dominate water–carbon coupling over physiological water-use efficiency at timescales beyond daily.

1 Introduction

Terrestrial carbon uptake by plants is the most variable component of interannual carbon cycle dynamics globally, taking up one-third of anthropogenic emissions annually (Lai et al., 2024; Prentice et al., 2024; Friedlingstein et al., 2026). This variability is the primary source of uncertainty in predictions of atmospheric carbon (James T. Randerson et al., 2025; Friedlingstein et al., 2026). However, because primary productivity cannot be directly measured at scale, estimates of carbon cycle dynamics and feedbacks rely on proxy-based methods and accounting approaches (Ruehr et al., 2023; James T. Randerson et al., 2025; Friedlingstein et al., 2026).

https://doi.org/10.5194/egusphere-2026-3250
Preprint. Discussion started: 30 July 2026

Because the terrestrial water and carbon cycles are tightly coupled, changes in one drive changes in the other (Novick et al., 2018; Piao et al., 2020; Humphrey et al., 2021; Yang et al., 2023). This coupling means that information about water availability can help constrain carbon cycle predictions, and vice versa (Seneviratne et al., 2010; Short Gianotti et al., 2019; Short Gianotti and Entekhabi, 2024), which has led to frequent use of the global water cycle as an explanatory variable for retrospective and predictive carbon cycle estimates (Poulter et al., 2014; Ahlström et al., 2015; Stocker et al., 2018; Trugman et al., 2018; Humphrey et al., 2021; Feldman et al., 2024; Green, 2024; Green et al., 2024), and vice versa (Eagleson, 1978b; Swann et al., 2012; Zhu et al., 2017; Kooperman et al., 2018; Lemordant et al., 2018; Zeng et al., 2018; Piao et al., 2020; Giardina et al., 2023; Yang et al., 2023; Green et al., 2024; Cordak et al., 2025). Disentangling these mechanisms across space and time is essential for constraining carbon cycle predictions and understanding climate feedbacks.

1.1 Functional Water–Productivity Relationships

Historically, the study of spatial productivity–water relationships has centered on rain-use efficiency (RUE = precipitation/net primary production), reflecting water's recognized role as a landscape-scale control on plant growth (Walter, 1939; Sala et al., 1988; Lauenroth and Sala, 1992; Knapp et al., 2017). However, RUE relationships show high site-to-site variability and poor convergence across biomes (Figure 1a), likely because plants respond mechanistically to soil moisture and vapor pressure deficit rather than precipitation itself (Wang et al., 2026). Recently, water-use efficiency metrics based on evapotranspiration (ET) have shown stronger convergence (Biederman et al., 2016), and in particular, the relationship between GPP and evaporative fraction (EF = latent heat flux / available energy) has been shown to be more consistent across sites and climates (Short Gianotti and Entekhabi, 2024). We use EF here because it (1) is mechanistically closer to plant responses, (2) normalizes for surface energy budget effects across latitude and climate gradients, and (3) shows convergent relationships across biomes at monthly timescales. A detailed review of RUE and water-use efficiency literature is provided in Supplementary Material Section 1.

1.2 Approach

Here, we investigate whether water–carbon coupling is driven by structural processes (canopy extent) or by physiological processes (canopy-averaged water-use efficiency). Specifically, we test the hypothesis that canopy fractional cover (f_v) is the primary mechanism linking water availability to productivity at subseasonal-to-seasonal timescales.

This hypothesis rests on two observations. First, leaf area responds consistently to water availability across bioclimates, independent of plant functional type (Li et al., 2022). If landscape-scale productivity–water relationships are biome-independent, then structural mechanisms must dominate over trait-specific physiological mechanisms. Second, physiological responses (stomatal conductance, photosynthetic regulation) operate at sub-daily timescales (Schymanski et al., 2013; Franks et al., 2017), whereas structural changes (growth, leaf turnover, drought response) occur over days-to-weeks. Thus, at monthly timescales, physiological processes should be regularly in quasi-equilibrium with water variables, while structural dynamics continue to adjust.

https://doi.org/10.5194/egusphere-2026-3250
Preprint. Discussion started: 30 July 2026

We show that structural and physiological dynamics operate in tension across timescales: both amplify GPP increases after rain at daily scales, but at monthly scales they pull the GPP–EF relationship in opposite directions. Structural processes dominate the long-term spatial and temporal water–carbon coupling, suggesting that daily-scale correlations cannot be extrapolated to longer timescales without accounting for this timescale-dependent reversal.

2 Materials and Methods

2.1 Conceptual Framework

To test the hypothesis that canopy fractional cover drives water–carbon coupling, we use a mathematical framework that explicitly separates landscape-scale carbon fluxes into their structural (extensive) and physiological (intensive) components.

2.1.1 Landscape versus Canopy-Scale Fluxes

Carbon assimilation by plants (GPP) can be expressed in two ways: as landscape-level GPP (GPP_l), the total carbon uptake per land area including bare soil, or canopy-level GPP (GPP_c), the carbon uptake per vegetated area. This distinction matters because *intensive* properties like photosynthetic rate per leaf do not scale linearly to extensive properties like total landscape productivity, particularly when the intensive variable and the extent both respond dynamically to other drivers. Similarly, the total above-ground biomass and the total leaf area over a pixel, plot, or region integrate over plants or plant area, and so are proportional to (a) the changing size of the canopy, (b) the canopy-averaged quantities, and (c) their dynamic co-variation.

Using these definitions, landscape and canopy-level GPP are related as:

$$GPP_l = f_v GPP_c \tag{1}$$

where f_v is vegetation cover fraction (0 = bare soil, 1 = fully vegetated). We use this simple two-state model because it allows us to isolate the extensive (f_v) and intensive (GPP_c) components of productivity.

Note that GPP_c reflects average canopy photosynthetic rate; GPP_l depends on both this rate and canopy extent. Unless otherwise noted, GPP refers to GPP_l throughout.

2.1.2 Water-Use Efficiency

Following this framework, we define canopy water-use efficiency (all processes occur over vegetated fraction f_v):

$$\omega_c = \frac{GPP_c}{T_c} \tag{2}$$

where T_c is the transpired water per unit canopy area and ω_c is the canopy carbon assimilation divided by the canopy transpiration. Note that this is the same at the landscape scale, $\omega_l = (f_v GPP_c)/(f_v T_c) = \omega_c$ when calculated using only transpiration, but differs from common uses of "landscape WUE" or "ecosystem WUE" (often defined as $GPP_l/ET_l = f_v GPP_c/ET_l$, including bare soil evaporation to comprise landscape evapotranspiration, ET_l).

https://doi.org/10.5194/egusphere-2026-3250
Preprint. Discussion started: 30 July 2026

Combining Equations 1 and 2, we can write

$$GPP_l = f_v \cdot \omega_c \cdot ET_l \cdot \phi \qquad \text{where} \qquad \phi = \frac{T_c}{ET_l} \tag{3}$$

The T/ET ratio commonly cited in the literature is related to ϕ as follows:

$$\text{“T/ET ratio”} = \frac{T_l}{ET_l} = \frac{f_v T_c}{ET_l} = f_v \phi \tag{4}$$

This makes explicit that the “T” in T/ET includes both intensive (leaf-level) transpiration and extensive (vegetation amount) effects. Note that ϕ is rarely measured directly, but is an intensive variable, as a ratio of two other intensive variables. A detailed discussion is provided in Supplementary Material Section 2.

Because ϕ and ω_c are rarely measured directly, we calculate their product ($\omega_c \phi$) as:

$$\omega_c \phi = \mathrm{GPP}_l / (f_v \cdot \mathrm{ET}_l) \qquad \text{[units: } g_C \text{ / } g_{H_2O}\text{]} \tag{5}$$

Throughout the manuscript, we refer to $\omega_c \phi$ dynamics as “physiological” or “intensive” processes, in contrast to “structural” or “extensive” (f_v) processes.

2.2 Data Sources

2.2.1 Eddy Covariance Data

The primary data in this study come from measurements made at flux towers using eddy covariance methods (Baldocchi et al., 2001; Novick et al., 2018; Pastorello et al., 2020; Chu et al., 2023), specifically from the FLUXNET network and the AmeriFlux network (BASE and FLUXNET SUBSET datasets) (Boden et al., 2013; Pastorello et al., 2020; Chu et al., 2023). Specifics on individual variables (EF and GPP) are discussed in Supplemental Text S3. Details for each tower site are presented in Supplemental Table 1. Citations for each site’s data are in Supplemental Section 9.

2.2.2 MODIS Vegetation Data

We derive vegetation cover fraction f_v from MODIS/Terra Leaf Area Index (Myneni et al., 2021, LAI; version MCD15A3H; 4-day resolution, 500 m pixels) using the methods of Xiao et al. (2016) and landcover-specific clumping indices from He et al. (2012). When first differences of f_v are necessary, we use the slope between two neighboring 4-day f_v values.

2.2.3 Interstorm Drydowns

We flag days with less than 0.254 mm (“trace”) precipitation as interstorm “dry” days. After any day with greater than trace precipitation, we label the following consecutive days without rain a *drydown*. For some analyses we look only at daily dynamics within drydowns (explicitly stated).

https://doi.org/10.5194/egusphere-2026-3250
Preprint. Discussion started: 30 July 2026

Variable	Name	Units	Notes
f_v	Fractional Vegetation Cover	–	
LE	Latent Heat Flux	$\mathrm{W\,m^{-2}}$	$LE = \lambda ET_l$, for latent heat of vaporization λ
H	Sensible Heat Flux	$\mathrm{W\,m^{-2}}$	Turbulent available energy $A = H + LE$
EF	Evaporative Fraction	–	Ratio of landscape/averaged latent heat flux to landscape averaged available energy $EF = \frac{LE}{A}$
T_c	Transpiration	$\mathrm{kg_{H_2O}\,m^{-2}\,s^{-1}}$	Transpired water flux through the canopy area fraction f_v
GPP_c	Canopy Gross Primary Productivity	$\mathrm{g_C\,m^{-2}\,day^{-1}}$	Carbon uptake rate per canopy area
GPP_l	Landscape Gross Primary Productivity	$\mathrm{g_C\,m^{-2}\,day^{-1}}$	Carbon uptake rate averaged over an entire (partially/vegetated) landscape
ω_c	Canopy-Averaged Water-Use Efficiency	$\mathrm{g_C\,g_{H_2O}^{-1}}$	Ratio of canopy/averaged carbon uptake to canopy-averaged transpired water
ϕ	Transpiration Intensity Ratio	–	Ratio of (intensive) canopy/averaged transpiration rate to landscape-averaged evapotranspiration rate

Table 1. Variables and abbreviations used in this study.

2.3 Methods

2.3.1 Non-Parametric Curves

To fit curves to data points for visualization, we use a montone copula smoother which projects all data points onto the 1:1 quantile line, and is agnostic with respect to independent/dependent variables (Short Gianotti, 2025, see Supplemental Materials).

https://doi.org/10.5194/egusphere-2026-3250
Preprint. Discussion started: 30 July 2026

2.3.2 Dynamical System Estimation

We use regression-based dynamical systems models to show trajectories within phase spaces (Figure 4). For each 2D dynamical system, we fit a system of first-order autonomous differential equations of the following form:

$$\begin{aligned} \frac{\mathrm{dEF}}{\mathrm{d}t} &= a_1 + a_2\mathrm{EF} + a_3\mathrm{GPP}_l + a_4\mathrm{EF}^2 + a_5\mathrm{GPP}_l^2 + a_6\mathrm{EF}\cdot\mathrm{GPP}_l \\ \frac{\mathrm{dGPP}_l}{\mathrm{d}t} &= b_1 + b_2\mathrm{EF} + b_3\mathrm{GPP}_l + b_4\mathrm{EF}^2 + b_5\mathrm{GPP}_l^2 + b_6\mathrm{EF}\cdot\mathrm{GPP}_l \end{aligned} \tag{6}$$

This is a generic 1st-order nonlinear (quadratic) time-invariant dynamical system, which is fit using ordinary least-squares. For further details see Supplemental Section 6.

2.3.3 Monthly Linear Regressions

Monthly linear regressions are estimated using monthly mean values of the variables (all days regardless of precipitation), using only growing season months and ordinary least-squares. Any month with fewer than 25 daily observations for a specified variable is discarded for that site, and any site with less than 6 complete months is discarded as well. Growing season is defined as months with $\geq 10\%$ of the site's maximum observed monthly GPP.

3 Results

3.1 Form of the Productivity–Water Relationship

Figure 1 compares two water–productivity relationships. Panel 1a shows the relationship between monthly precipitation and landscape GPP during the growing season at three representative sites: US-Seg (Litvak, 2016; Cunliffe et al., 2022), AU-DaS (Hutley et al., 2011), and US-Ne3 (Andy Suyker, 2025; Malek-Madani et al., 2020). This is the gross productivity analog to the rain-use efficiency (RUE) metric, which relates annual precipitation to net primary productivity (Supplemental Figure 1). All growing season months are shown. The blue lines show local non-parametric curve fits to the GPP–precipitation observations, which are agnostic to independent/dependent variable designation, and which explain 8.9, 38.4, and 2.7% of the variance in GPP (11.8, 44.4, 2.7% of precipitation) respectively.

The grey line shows the equivalent curve fit for all 271 sites used in these analyses, and explains 9.2, 42.2, and 1.6% of GPP variance in the three sites shown (8.8, 36.5, 1.9% of precipitation). Across all sites, the grey curve explains 6.4% (2.8%) of the full variance in GPP across all monthly observations for all sites and 12.8% (11.5%) on average by site. Every one of these metrics is worse for the NPP–precipitation except for the local curve fit for US-Ne3 which explains 8.1% of local GPP variance. The curve-fit relating monthly tower precipitation and NPP across all sites explains less than 1% of the variance in either variable.

Figure 1b shows the GPP–EF relationships for the same sites between monthly landscape GPP and EF. In all cases, a roughly monotonic, non-linear relationship exists between GPP and EF. The local curves explain 43.3, 77.7, and 47.9% of the monthly variability in GPP (40.3, 83.3, and 65.5 for EF). The grey curve fit to all months at all sites explains 52.1 (47.0), 79.4 (80.0),

https://doi.org/10.5194/egusphere-2026-3250
Preprint. Discussion started: 30 July 2026

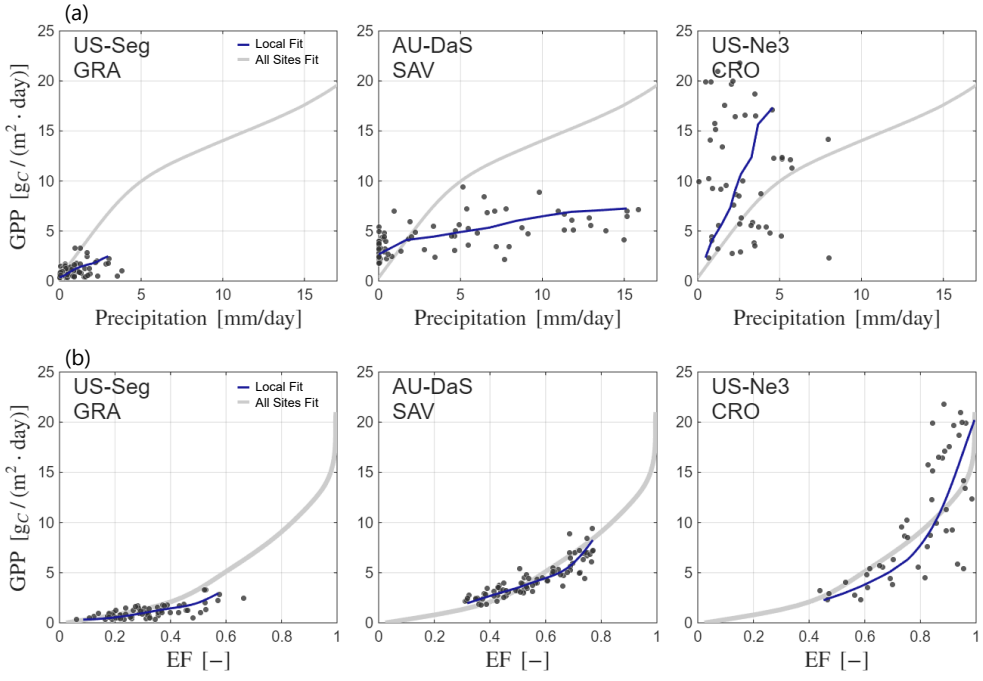

Figure 1. Two previously proposed productivity–water relationships at three sites. (a) Plots of monthly landscape-level Gross Primary Productivity (GPP_l) versus monthly-averaged precipitation rate (ratio is rain-use efficiency) at three eddy covariance flux tower sites: Sevilleta Grassland (US-Seg), Daly River Savanna (AU-DaS), and Mead (US-Ne3). Markers show all monthly values of GPP and precipitation during the growing season, defined as any month with more than 10% of long-term maximum monthly GPP. Local and All-Sites ($n = 271$ sites) curves are non-parameteric and impartial to independent/dependent variable designation. (b) Monthly (GPP_l) versus monthly Evaporative Fraction (EF) during the growing season for the same sites. The rain-use efficiency relationship in (a) shows highly variable relationships at and across sites (Huxman et al., 2004a; Knapp et al., 2017), while the GPP–EF relationship investigated here shows convergence across sites to the same monthly dynamics (Short Gianotti and Entekhabi, 2024; Short Gianotti et al., 2024). See Supplemental Figure S1 for ANPP-preciptation relationship.

https://doi.org/10.5194/egusphere-2026-3250
Preprint. Discussion started: 30 July 2026

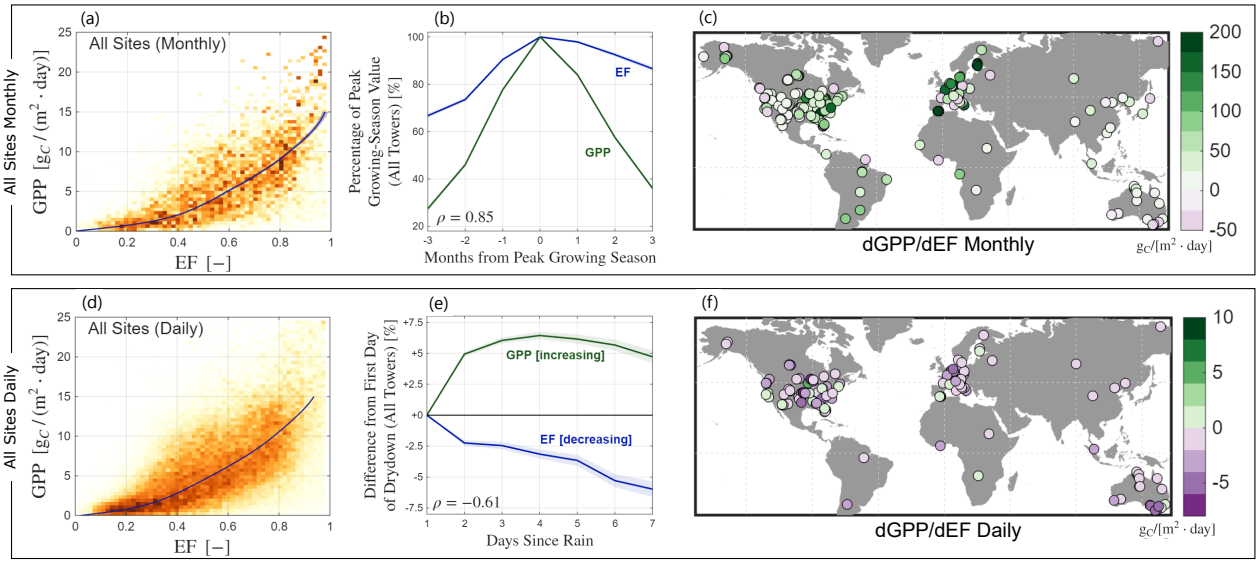

Figure 2. General relationship between landscape Gross Primary Productivity (GPP_l) and Evaporative Fraction (EF) at monthly and daily scales. (a) The joint density of all monthly GPP and EF during the local growing season across all 271 sites. Black line shows non-parametric fit to all monthly points. (b) Monthly GPP and EF relative to local annual peak value for all months, all towers ($n = 11,776$ months). y-axis scaling is relative to the local mean GPP or EF for the month of year with highest climatological GPP, and x-coordinate is relative to that month. Lines show averages of all monthly percentages across all years and all sites ($1,445 \leq n \leq 1,709$ for each point). Shading shows $\pm$ 1 standard error in means (very narrow due to sample size). EF is at its local peak when GPP is at its peak; both variables co-evolve with *positive* monthly correlation into and out of peak growing season. (c) Map of $d\mathrm{GPP}_l/d\mathrm{EF}$ estimated by linear regression for all towers (mean 51 $\mathrm{g_C\,m^{-2}\,day^{-1}}$), higher in wetter climates, significantly greater than 0 at 87% of sites. (d) The joint density of daily GPP and EF across all towers. Black line shows non-parametric fit to all daily points. (e) The percent increase (decrease) in daily GPP (EF) for days immediately following rainfall. Shading shows standard error in means across all sites and all growing season days following rain. GPP broadly increases in the week after local rain events, and EF broadly decreases. (f) Map of median $d\mathrm{GPP}_l/d\mathrm{EF}$ for days 1 and 2 after all rain events by site (mean $-1.2\,\mathrm{g_C\,m^{-2}\,day^{-1}}$), more *negative* in wetter climates, significantly less than 0 at 86% of sites.

and 53.3 (64.7)% of the GPP (EF) variance at the three sites, 28.9 (34.2) % of GPP (EF) across all sites, all months, and 32.5 (27.8)% when averaged across sites, substantially higher than the precipitation-based relationship, and sufficient to detect convergence patterns. See Supplemental Figure 2 for all individual site curves.

3.1.1 Monthly Scales: Positive Correlation

Figure 2 shows the temporal and spatio-temporal relationships between GPP and EF at different timescales. Monthly GPP and EF values for all towers are jointly distributed with a positive, non-linear correlation structure, both within and across sites (c.f. Huxman et al., 2004a; Biederman et al., 2016; Knapp et al., 2017). Figure 2a shows the joint distribution of these

https://doi.org/10.5194/egusphere-2026-3250
Preprint. Discussion started: 30 July 2026

two variables for all monthly growing-season observations (n=11,776 monthly observations) at all 271 tower sites. The relationship is convex, with $d\mathrm{GPP}_l/d\mathrm{EF} > 0$ in general across all monthly data. The dark line shows a representative curve for the monthly observations using the same method as Figure 1, with 99% confidence intervals (shaded region) calculated from 10,000 bootstrap resamplings. The narrow intervals reflect the large sample size and strong signal.

Figure 2c maps the monthly $d\mathrm{GPP}_l/d\mathrm{EF}$ for each site, calculated as the Sen-slope of a local linear fit to all growing season months. Slopes are mostly positive (87%), as are the mean (51 $\mathrm{g_C\,m^{-2}\,day^{-1}}$) and the median (31 $\mathrm{g_C\,m^{-2}\,day^{-1}}$) across sites, with wetter, more vegetated biomes showing higher slopes.

3.1.2 Daily Scales: Negative Correlation

To investigate the dynamics of GPP and EF, we show how they evolve during interstorm drydowns. Figure 2d again shows the joint GPP–EF density, but now at daily scale for all growing season days across all sites (n = 325,374). These show a very similar convex relationship with higher values of GPP when and where EF is high. The dark blue non-parametric curve is calculated as in Figure 2a, but using all daily data, leading to even narrower confidence intervals in the median. Although the curve-fitting is indifferent to dependent/independent variable designation, the medians across the bootstrapped curves are taken across GPP values (y-axis) in both Figure 2a and d.

Still at daily scale, Figure 2e shows the typical changes in GPP and EF for the first seven days after rain events. Using all growing season drydowns from all tower sites, we calculate the day-to-day changes in GPP and EF. The percentage changes are calculated as the mean of $100 \times X(t)/X(1)$ for each of GPP and EF for each day. Daily GPP and EF show opposite-sign dynamics after rain. On average across sites GPP increases in the days after rain (Fig. 2e, green line), and EF decreases (blue line). This is the mechanics of the negative correlation between GPP and EF at daily timescale, opposite of the positive monthly relationships at most sites (2c), and opposite of the positive spatial biogeographic relationship using long-term means (Short Gianotti and Entekhabi, 2024).

EF decreases during drydowns as soil water is depleted by drainage and evapotranspiration, and available energy shifts from latent heat toward sensible heat (McColl et al., 2017; Feldman et al., 2019). In contrast, GPP increases after rain due to increased photosynthetically active radiation (PAR) from cloud clearance, stomatal opening in response to higher leaf water potential, and active photosynthetic up-regulation (Feldman et al., 2021a; Holtzman et al., 2024). Although bare soil evaporation and transpiration can increase after rain (Zhao et al., 2022), by normalizing by available energy, EF isolates water depletion signals and remains monotonic more so than ET.

Although the full joint GPP–EF distributions across time and sites are quite similar at daily and monthly scales (Fig. 2ad), their dynamic relationships are quite different (Fig. 2be and 2cf). While EF generally decreases in the days after rain, GPP increases (Fig. 2e), leading to negative $d\mathrm{GPP}_l/d\mathrm{EF}$ at daily scale (Figure 2f; mean, median for first two days after rain: -1.22, $-1.23\,\mathrm{g_C\,m^{-2}\,day^{-1}}$; for first five days: -0.49, $-0.54\,\mathrm{g_C\,m^{-2}\,day^{-1}}$). The positively-correlated relationship in Figure 2a is composed of positive monthly correlations at nearly all sites (Figure 2c). The similar-appearing joint density in Figure 2b is instead composed of thousands of co-evolutions of GPP and EF after rain with predominantly negative day-to-day correlations.

https://doi.org/10.5194/egusphere-2026-3250
Preprint. Discussion started: 30 July 2026

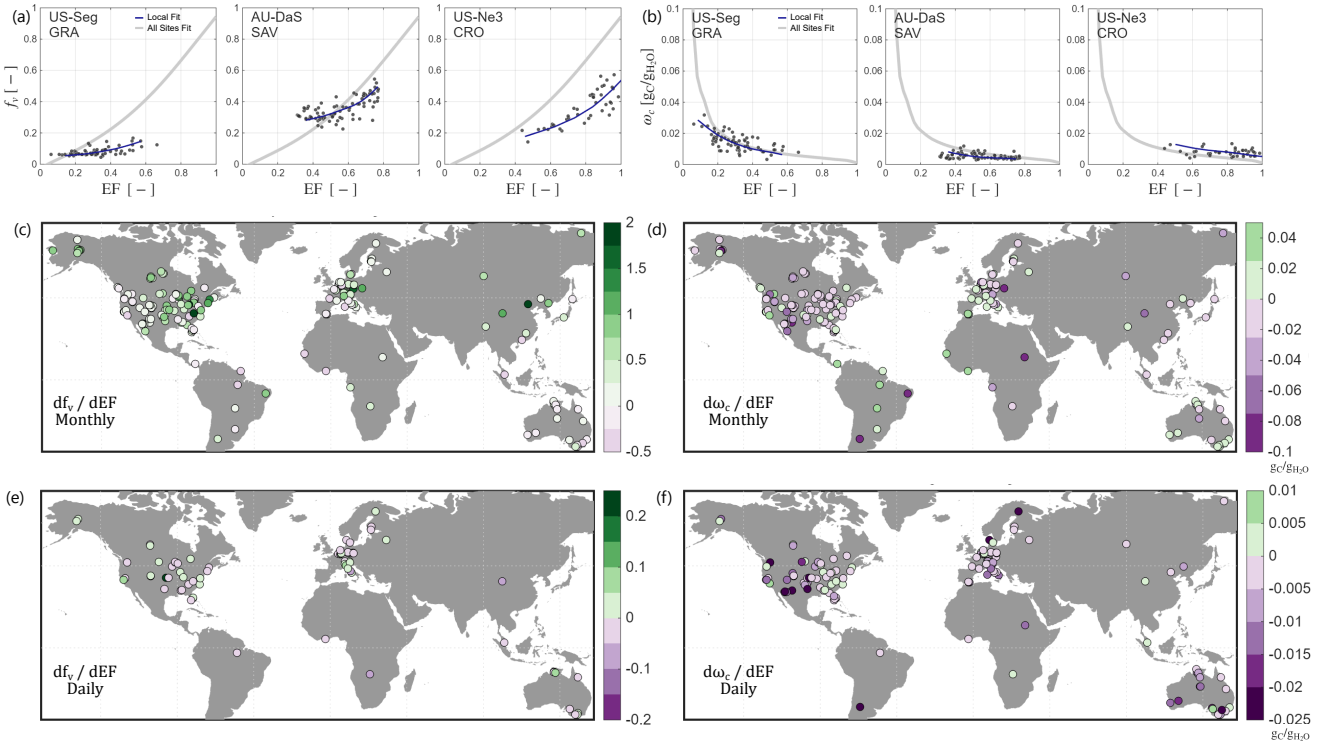

Figure 3. Structural and physiological contributions to landscape water–carbon dynamics. (a) Monthly relationships between landscape vegetation cover fraction (f_v) and EF for the same sites as in Fig. 1. f_v is *positively* correlated with EF (and GPP$_l$, not shown) at each site and across all sites for all months (grey all-sites fit), and convex like the GPP–EF relationship in Figure 1b. (b) Monthly relationships between physiological water-use component ($\omega_c\phi$) and EF for the same sites as in Fig. 1. $\omega_c\phi$ is exactly canopy-averaged water-use efficiency when soil evaporation (per area of bare soil) and transpiration rates (per canopy area) are equal at monthly scale. The intensive physiological term is *negatively*-correlated with EF (and GPP$_l$, not shown) at each site and across all sites for all months (grey All-Sites fit). (c) Map of $df_v/d\mathrm{EF}$ at monthly timescale as in Fig. 2c, predominantly greater than 0. (d) Map of $d\omega_c/d\mathrm{EF}$ at monthly timescale as in Fig. 2c, assuming $\phi = 1$, predominantly less than 0. (d) Map of $df_v/d\mathrm{EF}$ at daily timescale as in Fig. 2f, predominantly less than 0—the opposite sign of the f_v–EF relationship at monthly timescale (c), as is the case for the GPP–EF relationship. (f) Map of $d\omega_c/d\mathrm{EF}$ at daily timescale as in Fig. 2f, assuming $\phi = 1$ (see Supplemental Materials for discussion), predominantly less than 0. Unlike GPP and f_v, ω_c is nearly always negatively-correlated with EF across sites and timescales.

185 This sign reversal leads to a separation of timescales and indicates that daily trajectories represent movement toward the slow curve (grey line in Figure 1a, blue line in Figure 2a) that bridges monthly dynamics and spatial water–carbon states.

3.2 Structural and Physiological Components of Canopy Dynamics

Using Equation 3 ($\mathrm{GPP}_l = f_v\omega_c\phi\mathrm{ET}_l$) we decompose the GPP–EF dynamics into structural (f_v–EF) and physiological ($\omega_c\phi$–EF) components. Figure 3(a) shows monthly f_v–EF relationships at the same sites as in Figure 1. At all three sites and globally

https://doi.org/10.5194/egusphere-2026-3250
Preprint. Discussion started: 30 July 2026

(grey line) f_v and EF are positively-correlated and convex, the same pattern as GPP–EF (Figure 1b). This suggests that structural dynamics drive the overall GPP—EF relationship.

In contrast, the physiological component ($\omega_c\phi$) is negatively-correlated with EF at monthly scales (Figure 3b). Treating $\phi \approx 1$ (i.e., assuming bare soil and canopy evaporation rates per area are similar), ω_c decreases with increasing EF. This reveals competing mechanisms: structural dynamics (f_v) and physiological dynamics (ω_c) pull the GPP–EF relationship in *opposite* directions. However, the positive f_v–EF relationship dominates, and monthly GPP–EF dynamics follow canopy extent rather than water-use efficiency. Increases in GPP due to high water-use efficiency are negligible relative to structural dynamics.

3.2.1 Spatial Patterns

The f_v–EF slopes at monthly-scales are largest in humid, more-vegetated landscapes and smallest in arid regions (Figure 3c). The physiological slopes (Figure 3d) are opposite in sign, with the most negative values in arid regions. The daily physiological dynamics reinforce the monthly dynamics (Figure 3f), following textbook patterns from laboratory studies (Lambers and Oliveira, 2019a). The daily f_v–EF relationships are weak (mean $df_v/d\mathrm{EF} = -0.03$ for the first two days after rain, a 3% increase in f_v per day if EF were to decrease from 1 to 0), as might be expected from slow changes in canopy structure.

3.2.2 Resolving the Dynamics of the Two Timescales

The maximum-likelihood fit for Equation 6 for all daily data gives the following parameterized system:

$$\frac{d}{dt}\begin{bmatrix}\mathrm{EF}\\ \mathrm{GPP}_l\end{bmatrix} = \mathbf{B}\begin{bmatrix}1 & \mathrm{EF} & \mathrm{GPP}_l & \mathrm{EF}^2 & \mathrm{GPP}_l^2 & \mathrm{EF}\cdot\mathrm{GPP}_l\end{bmatrix}' \tag{7}$$

where $\mathbf{B} =$

$$10^{-4}\times\begin{bmatrix} 87.99\,[-] & 713.4\,[-] & 42.382\left[\frac{\mathrm{m^2\cdot day}}{\mathrm{g_C}}\right] & -3891\,[-] & -6.557\left[\frac{\mathrm{m^4\cdot day^2}}{\mathrm{g_C^2}}\right] & 229.2\left[\frac{\mathrm{m^2\cdot day}}{\mathrm{g_C}}\right] \\ 297.8\left[\frac{\mathrm{g_C}}{\mathrm{m^2\cdot day}}\right] & 1429\left[\frac{\mathrm{g_C}}{\mathrm{m^2\cdot day}}\right] & -207.6\,[-] & 2779\left[\frac{\mathrm{g_C}}{\mathrm{m^2\cdot day}}\right] & -36.21\left[\frac{\mathrm{m^2\cdot day}}{\mathrm{g_C}}\right] & 407.4\,[-] \end{bmatrix}$$

Because Eq. 7 is fit only within drydowns, the system is shocked by rain events (largely towards higher EF), and then evolves, initially with increasing GPP, f_v, and $\omega_c\phi$, and decreasing EF (Figs. 2f, 3ef). As the land surface, plants, and soils dry, EF decreases (leftward in phase space) while GPP increases, then both decline together toward the central "attractor" curve. This central curve represents the monthly-scale relationship (compare to Figure 2a) and the long-term biogeographical pattern (Figure 1b). These trajectories align with site-specifically estimated e-folding timescales in Short Gianotti et al. (2024), on the order of 3 days towards the attractor curve and 40 days along it for each site. Over weeks, GPP and f_v transition to positive correlations with EF as vegetation responds to sustained water limitation. This two-timescale evolution is shown in Figure 4a as vector flows in the GPP_l–EF phase space.

The dynamical system relationship is fit to gridded mean values of GPP, EF, $d\mathrm{GPP}/dt$, and $d\mathrm{EF}/dt$ to avoid underfitting less-sampled portions of the space and bioclimates with fewer flux towers. In the same spirit, the slow, attractor curve is fit

https://doi.org/10.5194/egusphere-2026-3250
Preprint. Discussion started: 30 July 2026

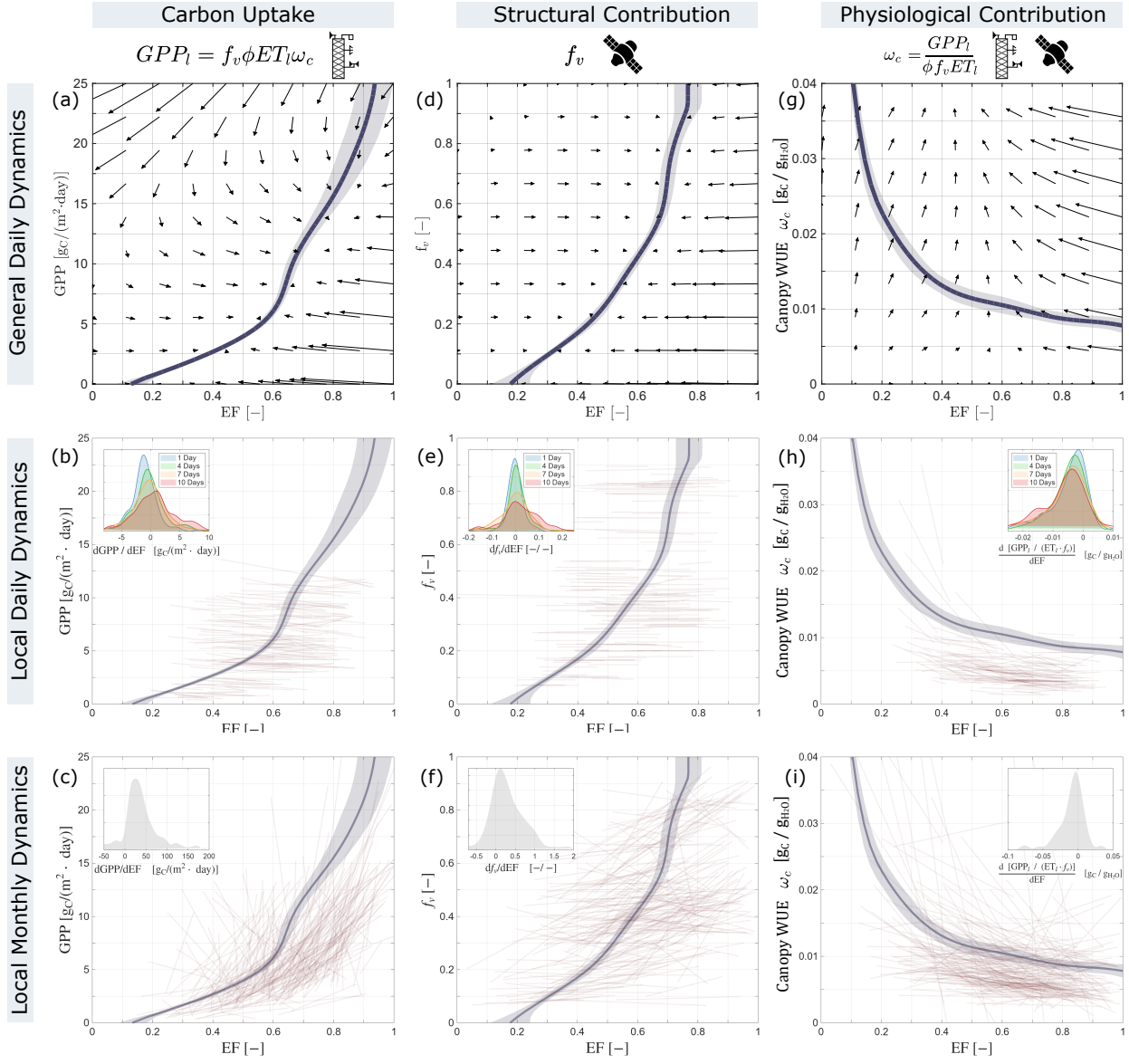

Figure 4. Dynamics of carbon uptake (tower GPP), landscape vegetation-cover fraction (satellite retrieved f_v), and residual water-use terms (calculated from tower and satellite data) versus EF. (a) Daily GPP–EF dynamics for all flux towers after rainfall (as in Figure 2e), system flow from Eq. 7. Curve and shading show the empirical mean daily growing-season GPP–EF relationship with equal weighting across the GPP–EF space and bootstrapped standard error, including rain days. (b) GPP–EF regressions for the first day after rain (day 2 minus day 1); each red line is a fit for a single tower site. Inset histogram shows the across-sites distribution of $d\mathrm{GPP}/d\mathrm{EF}$ slopes for the first 1, 4, 7, and 10 days post rain. Curve and shading as in 4a. (c) Linear regression fits for monthly-averaged GPP–EF values within the growing season, depicting slower sub-seasonal dynamics. Histogram shows across-site distribution of regression slopes. Curve and shading as in 4a. (d-f) Same as 4a-c, but with f_v–EF relationships. Flow dynamics from equivalent to Eq. 7, but fit using f_v and EF. (g-i) Same as 4a-c, but with ω_c–EF relationships, assuming equivalent bare soil and canopy evaporation rates. When $\phi = 1$, this is the canopy water-use efficiency, ω_c. Flow dynamics from equivalent to Eq. 7, but fit using ω_c and EF. Left column ordinate (GPP) is the product of the two following column ordinates ($f_v \cdot \omega_c \phi$) and ET_l (see Supplemental Figure 3 for ET_l–EF dynamics).

https://doi.org/10.5194/egusphere-2026-3250
Preprint. Discussion started: 30 July 2026

with weighting inversely proportional to the number of points per grid box, and then calculated as a binned mean across y-axis values. This process is then boot-strapped 10,000 times to create a 95% confidence interval which accounts for both the distribution of the data and for the potential effects of the gridding process. This curve is recreated in Figure 4b and c.

Wetter locations traverse paths nearer to the upper-right part of the phase space, while drier, less vegetated locations traverse more of the space in the lower left, but this can change with shifts in water supply (arid green-ups or forest droughts). Only after terrestrial systems approach the central curve of the global GPP–EF joint distribution (Figure 2ab) does GPP begin to decrease until further rain shocks the system, or other biophysical drivers lead to senescence and/or the end of the growing season (low GPP).

Figure 4b shows the typical relationships between GPP and EF immediately after rain events. Each red line is a linear fit to day 1–2 observations for a single site's drydowns (as in Figure 2f). Nearly all slopes are negative (median distribution in blue inset). As drydowns progress (green for day 4, orange for day 7, red for day 10), slopes gradually shift toward zero and then positive. This reflects the transition from photosynthetic up-regulation immediately post-rain to water-stress-driven down-regulation by day 10. At landscape-level, this transition period indicates that water stress develops gradually, not instantaneously.

At longer timescales still, the relationships between GPP and EF show predominantly positive correlations. Figure 4c shows linear regressions by site for each monthly-averaged value of GPP and EF (as in Figure 2c). These linear versions of the example curves in Figure 1b. At most sites, EF is higher in months when GPP is high, and vice versa. The inset histogram shows that typical slopes are positive, and with magnitudes a factor of 10 larger than for daily-scale relationships. Traversing the central curve on phenological timescales leads to large changes in GPP_l as would be intuitive from green-up and senescence processes.

The second column of Figure 4 shows the same analyses, but for the relationships between satellite-estimated f_v and tower EF. Figure 4d shows the daily dynamic flows, largely towards the central f_v–EF curve, estimated as in Figure 4a using all daily observations (weighted for equal phase-space sampling). As in Figure 4a, the mean curve is positively-sloped and convex, with lower EF and f_v values after long dry spells.

As in Figure 4b, Figure 4e shows the daily relationship at each site immediately after rain, but for the structural f_v–EF component of the GPP–EF relationship. The inset histogram shows that the f_v–EF slopes are more often negative than positive for the first days after rain (small increases in canopy extent); however, as drydowns progress and water stress increases, $\mathrm{d}f_v/\mathrm{dEF}$ becomes positive (day 7–10). This dynamics overturning is evidence of moisture pulses triggering visible canopy greening and sustained drying leading to visible canopy loss. The post-rain GPP–EF signals are more frequently significantly positive than f_v–EF in the first 1–2 days, which suggests that not all of the GPP increases in the first days of drydowns are caused by extensive increases in canopy structure and above-ground biomass. Some of these increases are also driven by increases in canopy-averaged photosynthesis through changes in absorbed light and/or increased average canopy conductance for carbon dioxide. Still, because the daily-scale f_v–EF slopes and the daily GPP–EF slopes share the same sign on average (Figures 4ad, 4be), increasing towards the central curve as EF decreases, some of the GPP increases coincide with structural canopy expansion.

https://doi.org/10.5194/egusphere-2026-3250
Preprint. Discussion started: 30 July 2026

Figure 4f shows the site-specific relationships between monthly f_v and EF. Like the GPP–EF relationships in Figure 4c, the majority of monthly correlations are positive, implying that all of GPP$_l$, f_v, and EF increase and decrease together in the growing season at nearly all sites at monthly scales. Again, the slopes are roughly an order of magnitude larger than their daily counterparts, pointing towards the larger role of slow canopy-extent processes in controlling water–carbon feedbacks relative to fast processes.

The third column of Figure 4 shows ω_c versus EF, where ω_c is calculated at daily scale as $\mathrm{GPP}_l/(f_v\mathrm{ET}_l)$, again assuming $\phi = 1$ (Eq. 2). Because the product $\omega_c\phi$ is not a commonly-used variable, we recommend interpreting these results through two lenses: (1) as the canopy water-use efficiency directly, i.e., assuming static ϕ or that ϕ is largely irrelevant to water–carbon coupling, and (2) as the convolution of coupled leaf-level WUE mechanisms (stomatal conductance dynamics and stress responses) with the daily changes in how bare soil evaporation and leaf transpiration differ. (1) requires an assumption which is strictly false, particularly in geographies with intermediate vegetation cover, but which we believe to be largely immaterial for qualitative interpretation.

Unlike f$_v$, the mean curve is negatively-sloped. $\omega_c\phi$ decreases at high EF (wet conditions) and increases at low EF (dry conditions). This pattern aligns with well-established leaf-level observations: plants become more water-use-efficient under water stress (Lambers and Oliveira, 2019b; Grossiord et al., 2020). Importantly, this means that at daily scales, both f_v and $\omega_c\phi$ increase immediately after rain, both contributing to GPP increases. But beyond weekly scales (Figure 4i), the negative $\omega_c\phi$–EF correlation remains, pulling the GPP–EF relationship downward, which the structural f_v dominance overcomes.

This opposing sign between $\omega_c\phi$ GPP dynamics is the key evidence for canopy structure's dominant role in GPP–EF coupling. Across all sites, GPP and f_v are positively correlated (median linear $\rho(\mathrm{GPP}_l, f_v) = 0.601$ at daily scales, 0.380 at monthly scales across sites), while GPP and $\omega_c\phi$ are only correlated for the first days after rain (median $\rho(\mathrm{GPP}_l, \omega_c\phi) = 0.578$ at daily scales, -0.18 at monthly scales). This apparent contradiction—that GPP decreases with the water-use efficiency term it's mathematically defined to be proportional to—arises because of f_v's negative covariance with $\omega_c\phi$. At monthly scales, wetter conditions have higher vegetation cover and lower canopy WUE, with the structural effect dominating the physiological effect on GPP.

Unlike the daily-scale dynamics in Figures 4be, the daily dynamics between EF and ω_c run roughly tangent to the mean curve—still with negative slopes. This implies that the intensive water-use changes lead to higher GPP as the land surface dries and EF goes down, as might be expected from a plant water conservation perspective. This amplifies the short term extensive greening seen between rain events in Figure 4e. Together, both Figures 4eh combine to drive increases in landscape GPP after rain events. Both could be thought of as positive feedbacks after rain: more vegetation is available to photosynthesize, and on average the vegetation becomes more efficient from a canopy-intensive water–carbon perspective. Notably, the negative slopes (driving GPP increases immediately after rain) become *more* negative as drydowns progress, with the mean slope magnitude increasing by roughly an order of magnitude over the first 10 days without rain (Figure 4h inset).

On monthly timescales (Figure 4i) the intensive properties also show a broadly negative correlation with EF. Unlike GPP and f_v, where longer dry periods without rain decrease extensive green vegetation cover and landscape GPP (Figures 4be), the intensive water-use properties act to increase GPP, or rather mitigate the GPP decreases. The intensive dynamics are a negative

https://doi.org/10.5194/egusphere-2026-3250
Preprint. Discussion started: 30 July 2026

(stabilizing) feedback on monthly scales, as opposed to extensive canopy dynamics which are aligned with GPP dynamics. The differences in slope magnitude, again roughly an order of magnitude between 1-day and 1-month timescales, are critical in the context of the time-varying optimization of intensive stomatal- and canopy-conductance models across biogeography and climatology (Holtzman et al., 2024).

The median linear correlation across sites between monthly GPP and monthly f_v is 0.69. The median linear correlation across sites between monthly GPP and monthly $\omega_c\phi$ is -0.28.

4 Discussion

The GPP–EF relationship shows stronger spatial convergence (roughly 30% of variance explained across all sites) than the commonly-used rain-use efficiency relationship (less than 1% of variance). This convergence is practically significant because: (1) EF is mechanistically relevant to plant responses (plants respond to and feed back on water availability), (2) EF is now widely measured at eddy covariance towers and estimable from standard weather station data (Rigden and Salvucci, 2015; McColl and Rigden, 2020), and (3) the convergent relationship suggests underlying ecological principles that could constrain models globally.

Structural Dynamics Dominate

Our results show that at timescales beyond daily, structural dynamics dominate water–carbon coupling. This suggests that models relying primarily on stomatal conductance or photosynthetic capacity to represent water–carbon feedbacks could misdiagnose the sign and magnitude of productivity responses to drought or increased water availability. Specifically, a water-stress-driven increase in water-use efficiency could be masked or reversed by concurrent decreases in f_v. Models must represent dynamic canopy extent (LAI, f_v) coupled to water availability, not just physiological processes. This emphasis on structural dynamics over physiology echoes earlier theories (Lauenroth and Sala, 1992; Paruelo et al., 1999), which identified vegetation extent and growth rate as primary mechanisms in precipitation–productivity relationships.

It is intuitive that the GPP–EF relationship follows a structural (f_v–EF) relationship: wet conditions favor more vegetation, which increases productivity. Less intuitive is that canopy-averaged water-use efficiency ($\omega_c\phi$) is negatively correlated with EF at all timescales. This negative correlation seems contradictory: GPP is defined to include $\omega_c\phi$ (Equation 3), yet GPP and $\omega_c\phi$ become negatively-correlated at monthly scales.

Physiological controls on water-use efficiency (stomatal conductance, photosynthetic regulation) operate at sub-daily timescales (minutes-to-hours), reaching quasi-equilibrium with local water availability within a day. At monthly timescales, these rapid physiological adjustments are averaged out, and their long-term values are emergent properties set by structural changes and phenological state. This timescale separation means that empirical water-use efficiency relationships calibrated from monthly or seasonal data may not extrapolate to novel conditions (e.g., elevated CO_2) without accounting for potential shifts in the canopy structural variables (f_v, LAI) that set the context in which physiology operates. This could bias future carbon cycle projections.

Water–Productivity Relationships are Timescale-Dependent

https://doi.org/10.5194/egusphere-2026-3250
Preprint. Discussion started: 30 July 2026

Many studies of productivity–water relationships highlight the need for multiple timescales to lead to the results they find (Lauenroth and Sala, 1992; Paruelo et al., 1999; Biederman et al., 2016). At sub-daily scales, physiological responses (stomatal conductance adjustments) reach quasi-equilibrium within hours. At daily-to-weekly scales, both physiological and structural processes operate, but structural responses are slower. At monthly-to-seasonal scales, only structural processes (growth, senescence, recruitment) produce observable changes in canopy extent, making them the dominant driver of landscape-scale productivity changes. At interannual-to-decadal scales, shifts in species composition and trait adaptation may become important again. This hierarchical structure implies that models calibrated at one timescale (e.g., leaf-chamber studies at hourly resolution) may not predict dynamics at another timescale (e.g., seasonal productivity). Conversely, empirical relationships like ours, which capture dynamics across multiple timescales (daily to monthly), may be more robust to extrapolation across conditions because they implicitly encode the time-varying importance of different mechanisms.

This also connects to phenological theory. A measurable amount of canopy expansion and leaf growth occurs in the first days after rain, and, conversely, *less* drought stress-induced leaf loss, branch turnover, and senescence occurs when it has just rained. This drives the tacit understanding that seasonal phenological evolution is comprised of—not distinct from—growth responses to resource availability at instantaneous timescales (Noy-Meir, 1973; Eagleson, 1978b; Feldman et al., 2018, 2021a, b; Wheeler and Dietze, 2023; Reich et al., 2025).

4.1 Limitations and Explanatory Variables

A key assumption in our analysis is that ϕ (the transpiration intensity ratio, $\mathrm{T}_c/\mathrm{ET}_l$) is approximately constant at 1. This assumption is poorly validated because direct measurements of ϕ are rare. However, at monthly timescales, ϕ likely becomes less variable as different evaporation pathways (bare soil, canopy interception, plant transpiration) average and converge to small values. Future work using sap flux measurements, isotopic partitioning, or empirical relationships could help validate this assumption and reveal whether ϕ varies systematically with climate or vegetation type (Rothfuss et al., 2010; Stoy et al., 2019).

We treat all vegetation globally with a single f_v–EF–GPP framework, ignoring differences in plant functional type, disturbance regime, population-level diversity. This is a deliberate simplification, justified by the convergence of the GPP–EF relationship across biomes (Figure 1b). However, this convergence could mask important differences in the mechanisms underlying structural and physiological responses across biomes. For instance, in deciduous versus evergreen systems, structural processes are radically different, even if their differences are small relative to the overall pattern (Short Gianotti and Entekhabi, 2024). Whether these mechanistic differences produce different coefficients in Equation 3, or whether the overall f_v–EF–GPP relationship is truly invariant across PFTs, remains unknown. Addressing this would require detailed partitioning of LAI changes into growth, senescence, and damage components, which current satellite data cannot provide. This represents an important frontier for multi-scale models combining remote sensing with ground-based phenology monitoring (e.g., PhenoCam, NEON).

We use vegetation cover fraction (f_v) as a proxy for canopy structural extent, but it has limitations. While a two-state subgrid model of bare soil and averaged-vegetation is a common, but simple, landscape-modeling approach, the two are never fully separable. Soils wet and dry beneath the canopy, and canopy interception and subsequent evaporation are major unconstrained

https://doi.org/10.5194/egusphere-2026-3250
Preprint. Discussion started: 30 July 2026

confounding variables (Miralles et al., 2010). The satellite-retrieved vegetation indices from which we estimate f_v are also imperfect (Zeng et al., 2023), tending to saturate in high vegetation contexts. To some degree using f_v rather than LAI itself helps with this issue, as it compresses the upper end of the range in still-interpretable ways. It is possible that looking at extensive vegetation properties might be better suited to a multi-scale approach, with higher spatial resolution extensive data which can then be aggregated to the tower scale. More nuanced future modeling studies could instead consider something closer to extensive landscape stomatal or chlorophyll counts or areas, or some more fine-grained relationship between the two.

Coupled Mechanisms

It would be incorrect to assume from these analyses that canopy extent "controls" EF or vice versa. Many previous studies have theorized about the directionality of productivity–water relationships (Noy-Meir, 1973; Lieth, 1975; Eagleson, 1978a, b; Williams and Albertson, 2005), and the coupling across timescales suggests the answer is almost certainly both.

Even with the evidence that the convergent GPP–EF relationship is explained primarily by a convergent f_v–EF relationship, these are empirical relationships rather than mechanistic or explicitly causal. There is a general tendency for EF to decrease after precipitation (Fig 2ef), which is mechanistically intuitive, but rarely fully modeled across all known underlying mechanisms (Dirmeyer et al., 2006; Ford et al., 2014; Haghighi et al., 2018). The tendency for greening over the course of days following rain events or rain sequences has some intuitive motivation, particularly in arid and semi-arid ecosystems, and has been demonstrated previously across the range of aridity (Reynolds et al., 2004; Huxman et al., 2004b; Chesson et al., 2004; Hilker et al., 2014; Feldman et al., 2018, 2021b; Lu et al., 2023; Feldman et al., 2024; Reich et al., 2025), although the covariance between precipitation and incoming shortwave radiation can mask the effect (Jonard et al., 2022). Still, this does not represent any of the complex underlying interactions between individual plants with water, plant-plant interactions, acclimation, carbohydrate allocation, atmospheric moisture advection, or even the absolute magnitude of evapotranspiration itself. Our convergent relationships suggest these mechanistic differences average out globally, but we cannot determine from this analysis whether the same processes dominate everywhere or whether different mechanisms produce similar large-scale patterns.

There are multiple existing hypotheses about the reasons behind this type of convergent behavior (Eagleson and Tellers, 1982; Farquhar and Sharkey, 1982; Reynolds and Chen, 1996; McConnaughay and Coleman, 1999; Mäkelä et al., 2002; Wright et al., 2003; Caylor et al., 2004; Harte et al., 2008; Dewar, 2010; Kleidon et al., 2010; del Jesus et al., 2012; Prentice et al., 2014; Wilcox et al., 2017; Joshi et al., 2022; Robinson, 2023; Prentice et al., 2024). One is that water-limited ecosystems converge toward an optimal trade-off between productivity and water conservation. Another hypothesis is that simple physics and stoichiometry of photosynthesis and transpiration produce convergent behaviors without requiring optimization. A third hypothesis is that the convergence is an evolutionary artifact: different mechanisms at different sites happen to produce similar large-scale patterns in response to multiple pressures. We cannot distinguish among these hypotheses from observational data alone. Future work combining process-based models (that encode mechanisms explicitly) with this empirical framework could help test which hypothesis is most consistent with observations.

Implications for Modeling

These analyses also address functional uncertainty in Land Surface Models and Earth System Models. Short Gianotti et al. (2024) showed that many models do not recreate the GPP_l–EF patterns seen here, suggesting calibration or dynamical differ-

https://doi.org/10.5194/egusphere-2026-3250
Preprint. Discussion started: 30 July 2026

ences. Because canopy extent's relationship with EF dominates the multi-day to seasonal GPP_l–EF relationship, the extensive canopy–water dynamic coupling (e.g., f_v, LAI) is the most likely source of discrepancy.

5 Conclusions

This study identifies the mechanisms coupling productivity (GPP) and water availability (EF) at two timescales. Daily dynamics are characterized by negative GPP–EF correlations due to changing weather states, physiological up-regulation responses, and non-negligible increases in canopy cover after rain. At monthly and longer timescales GPP transitions to positive correlation with EF, driven by structural changes in canopy extent (f_v). Structural dynamics are not only the primary driver at monthly scales, they overcome physiological mechanisms that would otherwise lead to *negative* monthly and spatial GPP–EF correlation.

We find that:

1. **Rain response:** Immediately after rainfall there is a broad tendency across biogeography for GPP to increase for days, leading to strong negative GPP–EF coupling in tower-based observations (Figure 2ef).

2. **Drydown dynamics:** As interstorm drydowns progress, GPP and EF evolve through their joint phase-space towards a convergent attractor curve with evolution time-scales of weeks, and which roughly follows the joint density of all daily growing observations across all sites, climates, and biomes (Figure 2ad).

3. **Monthly dynamics:** The monthly joint distribution of GPP and EF follows the attractor with positive correlations (Figure 2a). This suggests that the monthly relationship emerges from averaging daily drydown trajectories and shocks from precipitation, not from a distinct monthly process.

4. **Structural dominance at longer timescales:** Decomposing GPP into structural (f_v–EF) and physiological ($\omega_c\phi$–EF) components reveals their influence on the GPP–EF relationship. Because landscape GPP is directly proportional to both f_v and $\omega_c\phi$ by definition, if structural and physiological dynamics align, then GPP, f_v, and $\omega_c\phi$ will all evolve in the same direction with EF. This is only true at daily-scales. Beyond 10 day timescales, the f_v–EF relationship changes signs, and GPP follows the f_v dynamics rather than the physiological dynamics.

5. **Implications for biogeography and global patterns:** The convergence of the GPP–EF relationship across hundreds of sites and diverse biomes suggests that vegetation structural responses to water availability follow generalizable principles. Because canopy dynamics integrates both physiology and structural biology across timescales, the emergent GPP–EF relationship may be more robust for global projections than site-specific physiological models.

6. **Dynamic canopy representation in models:** Earth System Models that represent water-–carbon coupling using only stomatal conductance or photosynthetic capacity, without allowing canopy extent to properly respond to water availability, will misrepresent both the sign and magnitude of productivity feedbacks at monthly and longer scales. Models should

https://doi.org/10.5194/egusphere-2026-3250
Preprint. Discussion started: 30 July 2026

prioritize dynamic LAI/f_v coupled to soil moisture, which is likely a higher-impact improvement than refinements to physiological sub-models alone.

These results re-frame terrestrial water–carbon coupling as fundamentally a structural problem, how much vegetation is there and how does it respond to water availability, rather than a purely physiological problem of how efficiently individual leaves use water. This perspective suggests that at seasonal-to-interannual timescales, predicting productivity changes requires accurate representation of plant recruitment, mortality, and growth dynamics, not just photosynthetic capacity.

Data availability.

Flux tower data from AmeriFlux and FLUXNET networks are publicly available under CC-BY-4.0 licenses:

- AmeriFlux: https://ameriflux.lbl.gov/data
- FLUXNET: https://fluxnet.org/data/download-data/

Site-specific data sources and citations are provided in Supplementary Table 1 and Supplementary Material Section 9.

The MODIS/Terra+Aqua Leaf Area Index/FPAR 4-Day L4 Global 500m SIN Grid data (product MCD15A3H; version 061) are available through:

- LP DAAC: https://www.earthdata.nasa.gov/centers/lp-daac/data-access-tools
- NASA AppEEARS: https://appeears.earthdatacloud.nasa.gov/ (for site-level extraction)
- NASA EarthData Search: https://search.earthdata.nasa.gov/search (product: MCD15A3H)

Code for the monotone copula smoother (Figure fitting) is available at

- https://zenodo.org/records/17460263 (Short Gianotti, 2025).

Author contributions.

DJSG and DE were responsible for study conceptualization. DJSG performed the analyses, created the figures, and wrote the manuscript, DE provided feedback on analyses, manuscript structure, and figure creation. DJSG and DE edited the manuscript. DE provided funding and project management for the study.

Competing interests.

The authors declare no competing interests in this research.

https://doi.org/10.5194/egusphere-2026-3250
Preprint. Discussion started: 30 July 2026

Acknowledgements. The authors were funded in part by a NASA–Jet Propulsion Laboratory/California Institute of Technology subcontract (1,510,842) to the Massachusetts Institute of Technology

https://doi.org/10.5194/egusphere-2026-3250
Preprint. Discussion started: 30 July 2026

References

Ahlström, A., Raupach, M. R., Schurgers, G., Smith, B., Arneth, A., Jung, M., Reichstein, M., Canadell, J. G., Friedlingstein, P., Jain, A. K., Kato, E., Poulter, B., Sitch, S., Stocker, B. D., Viovy, N., Wang, Y. P., Wiltshire, A., Zaehle, S., and Zeng, N.: The Dominant Role of Semi-Arid Ecosystems in the Trend and Variability of the Land CO2 Sink, Science, 348, 895–899, https://doi.org/10.1126/science.aaa1668, 2015.

Andy Suyker: AmeriFlux BASE US-Ne3 Mead - Rainfed Maize-Soybean Rotation Site, https://doi.org/10.17190/AMF/1246086, 2025.

Baldocchi, D., Falge, E., Gu, L., Olson, R., Hollinger, D., Running, S., Anthoni, P., Bernhofer, C., Davis, K., Evans, R., Fuentes, J., Goldstein, A., Katul, G., Law, B., Lee, X., Malhi, Y., Meyers, T., Munger, W., Oechel, W., U, K. T. P., Pilegaard, K., Schmid, H. P., Valentini, R., Verma, S., Vesala, T., Wilson, K., and Wofsy, S.: FLUXNET: A New Tool to Study the Temporal and Spatial Variability of Ecosystem-Scale Carbon Dioxide, Water Vapor, and Energy Flux Densities, Bulletin of the American Meteorological Society, 82, 2415–2434, https://doi.org/10.1175/1520-0477(2001)082<2415:FANTTS>2.3.CO;2, 2001.

Biederman, J. A., Scott, R. L., Goulden, M. L., Vargas, R., Litvak, M. E., Kolb, T. E., Yepez, E. A., Oechel, W. C., Blanken, P. D., Bell, T. W., Garatuza-Payan, J., Maurer, G. E., Dore, S., and Burns, S. P.: Terrestrial Carbon Balance in a Drier World: The Effects of Water Availability in Southwestern North America, Global Change Biology, 22, 1867–1879, https://doi.org/10.1111/gcb.13222, 2016.

Boden, T. A., Krassovski, M., and Yang, B.: The AmeriFlux Data Activity and Data System: An Evolving Collection of Data Management Techniques, Tools, Products and Services, Geoscientific Instrumentation, Methods and Data Systems, 2, 165–176, https://doi.org/10.5194/gi-2-165-2013, 2013.

Caylor, K. K., Scanlon, T. M., and Rodriguez-Iturbe, I.: Feasible Optimality of Vegetation Patterns in River Basins, Geophysical Research Letters, 31, https://doi.org/10.1029/2004GL020260, 2004.

Chesson, P., Gebauer, R. L. E., Schwinning, S., Huntly, N., Wiegand, K., Ernest, M. S. K., Sher, A., Novoplansky, A., and Weltzin, J. F.: Resource Pulses, Species Interactions, and Diversity Maintenance in Arid and Semi-Arid Environments, Oecologia, 141, 236–253, https://doi.org/10.1007/s00442-004-1551-1, 2004.

Chu, H., Christianson, D. S., Cheah, Y. W., Pastorello, G., O'Brien, F., Geden, J., Ngo, S. T., Hollowgrass, R., Leibowitz, K., Beekwilder, N. F., Sandesh, M., Dengel, S., Chan, S. W., Santos, A., Delwiche, K., Yi, K., Buechner, C., Baldocchi, D., Papale, D., Keenan, T. F., Biraud, S. C., Agarwal, D. A., and Torn, M. S.: AmeriFlux BASE Data Pipeline to Support Network Growth and Data Sharing, Scientific Data, 10, 1–13, https://doi.org/10.1038/s41597-023-02531-2, 2023.

Cordak, A. S., Kooperman, G. J., Zarakas, C. M., Swann, A. L. S., and Koven, C. D.: The Role of Leaf Area Changes Within Plant CO2 Physiological Impacts on the Global Hydrological Cycle, Geophysical Research Letters, 52, e2024GL110 904, https://doi.org/10.1029/2024GL110904, 2025.

Cunliffe, A. M., Boschetti, F., Clement, R., Sitch, S., Anderson, K., Duman, T., Zhu, S., Schlumpf, M., Litvak, M. E., Brazier, R. E., and Hill, T. C.: Strong Correspondence in Evapotranspiration and Carbon Dioxide Fluxes Between Different Eddy Covariance Systems Enables Quantification of Landscape Heterogeneity in Dryland Fluxes, Journal of Geophysical Research: Biogeosciences, 127, e2021JG006 240, https://doi.org/10.1029/2021JG006240, 2022.

del Jesus, M., Foti, R., Rinaldo, A., and Rodriguez-Iturbe, I.: Maximum Entropy Production, Carbon Assimilation, and the Spatial Organization of Vegetation in River Basins, Proceedings of the National Academy of Sciences, 109, 20 837–20 841, https://doi.org/10.1073/pnas.1218636109, 2012.

https://doi.org/10.5194/egusphere-2026-3250
Preprint. Discussion started: 30 July 2026

Dewar, R. C.: Maximum Entropy Production and Plant Optimization Theories, Philosophical Transactions of the Royal Society B: Biological Sciences, 365, 1429–1435, https://doi.org/10.1098/rstb.2009.0293, 2010.

Dirmeyer, P. A., Koster, R. D., and Guo, Z.: Do Global Models Properly Represent the Feedback between Land and Atmosphere?, Journal of Hydrometeorology, 7, 1177–1198, https://doi.org/10.1175/JHM532.1, 2006.

Eagleson, P. S.: Climate, Soil, and Vegetation: 5. A Derived Distribution of Storm Surface Runoff, Water Resources Research, 14, 741–748, https://doi.org/10.1029/WR014i005p00741, 1978a.

Eagleson, P. S.: Climate, Soil, and Vegetation: 6. Dynamics of the Annual Water Balance, Water Resources Research, 14, 749–764, https://doi.org/10.1029/WR014i005p00749, 1978b.

Eagleson, P. S. and Tellers, T. E.: Ecological Optimality in Water-Limited Natural Soil-Vegetation Systems: 2. Tests and Applications, Water Resources Research, 18, 341–354, https://doi.org/10.1029/WR018i002p00341, 1982.

Farquhar, G. D. and Sharkey, T. D.: Stomatal Conductance and Photosynthesis, Annual Review of Plant Physiology, 33, 317–345, https://doi.org/10.1146/annurev.pp.33.060182.001533, 1982.

Feldman, A. F., Short Gianotti, D. J., Konings, A. G., McColl, K. A., Akbar, R., Salvucci, G. D., and Entekhabi, D.: Moisture Pulse-Reserve in the Soil-Plant Continuum Observed across Biomes, Nature Plants, 4, 1026–1033, https://doi.org/10.1038/s41477-018-0304-9, 2018.

Feldman, A. F., Short Gianotti, D. J., Trigo, I. F., Salvucci, G. D., and Entekhabi, D.: Satellite-Based Assessment of Land Surface Energy Partitioning–Soil Moisture Relationships and Effects of Confounding Variables, Water Resources Research, 55, 10 657–10 677, https://doi.org/10.1029/2019WR025874, 2019.

Feldman, A. F., Chulakadabba, A., Short Gianotti, D. J., and Entekhabi, D.: Landscape-Scale Plant Water Content and Carbon Flux Behavior Following Moisture Pulses: From Dryland to Mesic Environments, Water Resources Research, 57, e2020WR027 592, https://doi.org/10.1029/2020WR027592, 2021a.

Feldman, A. F., Short Gianotti, D. J., Konings, A. G., Gentine, P., and Entekhabi, D.: Patterns of Plant Rehydration and Growth Following Pulses of Soil Moisture Availability, Biogeosciences, 18, 831–847, https://doi.org/10.5194/bg-18-831-2021, 2021b.

Feldman, A. F., Konings, A. G., Gentine, P., Cattry, M., Wang, L., Smith, W. K., Biederman, J. A., Chatterjee, A., Joiner, J., and Poulter, B.: Large Global-Scale Vegetation Sensitivity to Daily Rainfall Variability, Nature, 636, 380–384, https://doi.org/10.1038/s41586-024-08232-z, 2024.

Ford, T. W., Wulff, C. O., and Quiring, S. M.: Assessment of Observed and Model-Derived Soil Moisture-Evaporative Fraction Relationships over the United States Southern Great Plains, Journal of Geophysical Research: Atmospheres, 119, 6279–6291, https://doi.org/10.1002/2014JD021490, 2014.

Franks, P. J., Berry, J. A., Lombardozzi, D. L., and Bonan, G. B.: Stomatal Function across Temporal and Spatial Scales: Deep-Time Trends, Land-Atmosphere Coupling and Global Models, Plant Physiology, 174, 583–602, https://doi.org/10.1104/pp.17.00287, 2017.

Friedlingstein, P., O'Sullivan, M., Jones, M. W., Andrew, R. M., Bakker, D. C. E., Hauck, J., Landschützer, P., Le Quéré, C., Li, H., Luijkx, I. T., Peters, G. P., Peters, W., Pongratz, J., Schwingshackl, C., Sitch, S., Canadell, J. G., Ciais, P., Aas, K., Alin, S. R., Anthoni, P., Barbero, L., Bates, N. R., Bellouin, N., Benoit-Cattin, A., Berghoff, C. F., Bernardello, R., Bopp, L., Brasika, I. B. M., Chamberlain, M. A., Chandra, N., Chevallier, F., Chini, L. P., Collier, N. O., Colligan, T. H., Cronin, M., Djeutchouang, L. M., Dou, X., Enright, M. P., Enyo, K., Erb, M., Evans, W., Feely, R. A., Feng, L., Ford, D. J., Foster, A., Fransner, F., Gasser, T., Gehlen, M., Gkritzalis, T., Goncalves De Souza, J., Grassi, G., Gregor, L., Gruber, N., Guenet, B., Gürses, Ö., Harrington, K., Harris, I., Heinke, J., Hurtt, G. C., Iida, Y., Ilyina, T., Ito, A., Jacobson, A. R., Jain, A. K., Jarníková, T., Jersild, A., Jiang, F., Jones, S. D., Kato, E., Keeling, R. F., Klein Goldewijk, K., Knauer, J., Kong, Y., Korsbakken, J. I., Koven, C., Kunimitsu, T., Lan, X., Liu, J., Liu, Z., Liu, Z., Lo Monaco, C., Ma, L., Marland,

https://doi.org/10.5194/egusphere-2026-3250
Preprint. Discussion started: 30 July 2026

G., McGuire, P. C., McKinley, G. A., Melton, J. R., Monacci, N., Monier, E., Morgan, E. J., Munro, D. R., Müller, J. D., Nakaoka, S.-I., Nayagam, L. R., Niwa, Y., Nutzel, T., Olsen, A., Omar, A. M., Pan, N., Pandey, S., Pierrot, D., Qin, Z., Regnier, P., Rehder, G., Resplandy, L., Roobaert, A., Rosan, T. M., Rödenbeck, C., Schwinger, J., Skjelvan, I., Smallman, T. L., Spada, V., Sreeush, M. G., Sun, Q., Sutton, A. J., Sweeney, C., Swingedouw, D., Séférian, R., Takao, S., Tatebe, H., Tian, H., Tian, X., Tilbrook, B., Tsujino, H., Tubiello, F., van Ooijen, E., van der Werf, G. R., van de Velde, S. J., Walker, A. P., Wanninkhof, R., Yang, X., Yuan, W., Yue, X., and Zeng, J.: Global Carbon Budget 2025, Earth System Science Data, 18, 3211–3288, https://doi.org/10.5194/essd-18-3211-2026, 2026.

Giardina, F., Gentine, P., Konings, A. G., Seneviratne, S. I., and Stocker, B. D.: Diagnosing Evapotranspiration Responses to Water Deficit across Biomes Using Deep Learning, New Phytologist, 240, 968–983, https://doi.org/10.1111/nph.19197, 2023.

Green, J. K.: The Intricacies of Vegetation Responses to Changing Moisture Conditions, New Phytologist, 244, 2156–2162, https://doi.org/10.1111/nph.20182, 2024.

Green, J. K., Zhang, Y., Luo, X., and Keenan, T. F.: Systematic Underestimation of Canopy Conductance Sensitivity to Drought by Earth System Models, AGU Advances, 5, e2023AV001 026, https://doi.org/10.1029/2023AV001026, 2024.

Grossiord, C., Buckley, T. N., Cernusak, L. A., Novick, K. A., Poulter, B., Siegwolf, R. T. W., Sperry, J. S., and McDowell, N. G.: Plant Responses to Rising Vapor Pressure Deficit, New Phytologist, 226, 1550–1566, https://doi.org/10.1111/nph.16485, 2020.

Haghighi, E., Short Gianotti, D. J., Akbar, R., Salvucci, G. D., and Entekhabi, D.: Soil and Atmospheric Controls on the Land Surface Energy Balance: A Generalized Framework for Distinguishing Moisture-Limited and Energy-Limited Evaporation Regimes, Water Resources Research, 54, 1831–1851, https://doi.org/10.1002/2017WR021729, 2018.

Harte, J., Zillio, T., Conlisk, E., and Smith, A. B.: Maximum Entropy and the State-Variable Approach to Macroecology, Ecology, 89, 2700–2711, https://doi.org/10.1890/07-1369.1, 2008.

He, L., Chen, J. M., Pisek, J., Schaaf, C. B., and Strahler, A. H.: Global Clumping Index Map Derived from the MODIS BRDF Product, Remote Sensing of Environment, 119, 118–130, https://doi.org/10.1016/j.rse.2011.12.008, 2012.

Hilker, T., Lyapustin, A. I., Tucker, C. J., Hall, F. G., Myneni, R. B., Wang, Y., Bi, J., Mendes de Moura, Y., and Sellers, P. J.: Vegetation Dynamics and Rainfall Sensitivity of the Amazon, Proceedings of the National Academy of Sciences, 111, 16 041–16 046, https://doi.org/10.1073/pnas.1404870111, 2014.

Holtzman, N., Sloan, B., Potkay, A., Katul, G., Feng, X., and Konings, A. G.: Ecosystem Water-Saving Timescale Varies Spatially With Typical Drydown Length, AGU Advances, 5, e2023AV001 113, https://doi.org/10.1029/2023AV001113, 2024.

Humphrey, V., Berg, A., Ciais, P., Gentine, P., Jung, M., Reichstein, M., Seneviratne, S. I., and Frankenberg, C.: Soil Moisture–Atmosphere Feedback Dominates Land Carbon Uptake Variability, Nature, 592, 65–69, https://doi.org/10.1038/s41586-021-03325-5, 2021.

Hutley, L. B., Beringer, J., Isaac, P. R., Hacker, J. M., and Cernusak, L. A.: A Sub-Continental Scale Living Laboratory: Spatial Patterns of Savanna Vegetation over a Rainfall Gradient in Northern Australia, Agric. For. Meteorol., 151, 1417–1428, 2011.

Huxman, T. E., Smith, M. D., Fay, P. A., Knapp, A. K., Shaw, M. R., Loik, M. E., Smith, S. D., Tissue, D. T., Zak, J. C., Weltzin, J. F., Pockman, W. T., Sala, O. E., Haddad, B. M., Harte, J., Koch, G. W., Schwinning, S., Small, E. E., and Williams, D. G.: Convergence across Biomes to a Common Rain-Use Efficiency, Nature, 429, 651–654, https://doi.org/10.1038/nature02561, 2004a.

Huxman, T. E., Snyder, K. A., Tissue, D., Leffler, A. J., Ogle, K., Pockman, W. T., Sandquist, D. R., Potts, D. L., and Schwinning, S.: Precipitation Pulses and Carbon Fluxes in Semiarid and Arid Ecosystems, Oecologia, 141, 254–268, https://doi.org/10.1007/s00442-004-1682-4, 2004b.

https://doi.org/10.5194/egusphere-2026-3250
Preprint. Discussion started: 30 July 2026

James T. Randerson, Yue Li, Weiwei Fu, Francois Primeau, Jinhyuk E. Kim, Mingquan Mu, Forrest M. Hoffman, Linqing Yang, Chao Wu, Jonathan A. Wang, William R. L. Anderegg, Mark A. Friedl, Sassan S. Saatchi, A. Scott Denning, and Michael L. Goulden: The Weak Land Carbon Sink Hypothesis, Science Advances, 10, 1–17, https://doi.org/10.1126/sciadv.adr5489, 2025.

Jonard, F., Feldman, A. F., Short Gianotti, D. J., and Entekhabi, D.: Observed Water and Light Limitation across Global Ecosystems, Biogeosciences, 19, 5575–5590, https://doi.org/10.5194/bg-19-5575-2022, 2022.

Joshi, J., Stocker, B. D., Hofhansl, F., Zhou, S., Dieckmann, U., and Prentice, I. C.: Towards a Unified Theory of Plant Photosynthesis and Hydraulics, Nature Plants, 8, 1304–1316, https://doi.org/10.1038/s41477-022-01244-5, 2022.

Kleidon, A., Malhi, Y., and Cox, P. M.: Maximum Entropy Production in Environmental and Ecological Systems, Philosophical Transactions of the Royal Society B: Biological Sciences, 365, 1297–1302, https://doi.org/10.1098/rstb.2010.0018, 2010.

Knapp, A. K., Ciais, P., and Smith, M. D.: Reconciling Inconsistencies in Precipitation–Productivity Relationships: Implications for Climate Change, New Phytologist, 214, 41–47, https://doi.org/10.1111/nph.14381, 2017.

Kooperman, G. J., Fowler, M. D., Hoffman, F. M., Koven, C. D., Lindsay, K., Pritchard, M. S., Swann, A. L., and Randerson, J. T.: Plant Physiological Responses to Rising CO2 Modify Simulated Daily Runoff Intensity With Implications for Global-Scale Flood Risk Assessment, Geophysical Research Letters, 45, 12,457–12,466, https://doi.org/10.1029/2018GL079901, 2018.

Lai, J., Kooijmans, L. M. J., Sun, W., Lombardozzi, D., Campbell, J. E., Gu, L., Luo, Y., Kuai, L., and Sun, Y.: Terrestrial Photosynthesis Inferred from Plant Carbonyl Sulfide Uptake, Nature, 634, 855–861, https://doi.org/10.1038/s41586-024-08050-3, 2024.

Lambers, H. and Oliveira, R. S.: Plant Physiological Ecology, Springer International Publishing, Cham, ISBN 978-3-030-29638-4 978-3-030-29639-1, https://doi.org/10.1007/978-3-030-29639-1, 2019a.

Lambers, H. and Oliveira, R. S.: Plant Water Relations, in: Plant Physiological Ecology, edited by Lambers, H. and Oliveira, R. S., pp. 187–263, Springer International Publishing, Cham, ISBN 978-3-030-29639-1, https://doi.org/10.1007/978-3-030-29639-1_5, 2019b.

Lauenroth, W. K. and Sala, O. E.: Long-Term Forage Production of North American Shortgrass Steppe, Ecological Applications, 2, 397–403, https://doi.org/10.2307/1941874, 1992.

Lemordant, L., Gentine, P., Swann, A. S., Cook, B. I., and Scheff, J.: Critical Impact of Vegetation Physiology on the Continental Hydrologic Cycle in Response to Increasing CO2, Proceedings of the National Academy of Sciences of the United States of America, 115, 4093–4098, https://doi.org/10.1073/pnas.1720712115, 2018.

Li, W., Migliavacca, M., Forkel, M., Denissen, J. M. C., Reichstein, M., Yang, H., Duveiller, G., Weber, U., and Orth, R.: Widespread Increasing Vegetation Sensitivity to Soil Moisture, Nature Communications, 13, 3959, https://doi.org/10.1038/s41467-022-31667-9, 2022.

Lieth, H.: Modeling the Primary Productivity of the World, in: Primary Productivity of the Biosphere, edited by Jacobs, J., Lange, O. L., Olson, J. S., Wieser, W., Lieth, H., and Whittaker, R. H., vol. 14, pp. 237–263, Springer Berlin Heidelberg, Berlin, Heidelberg, ISBN 978-3-642-80915-6 978-3-642-80913-2, https://doi.org/10.1007/978-3-642-80913-2_12, 1975.

Litvak, M.: AmeriFlux US-Seg Sevilleta Grassland, Tech. rep., University of New Mexico, https://doi.org/10.17190/AMF/1246124, 2016.

Lu, Z., Chen, D., Wyser, K., Fuentes-Franco, R., Olin, S., Zhang, Q., Wu, M., and Ahlström, A.: Natural Decadal Variability of Global Vegetation Growth in Relation to Major Decadal Climate Modes, Environmental Research Letters, 18, 014 033, https://doi.org/10.1088/1748-9326/acacb4, 2023.

Mäkelä, A., Givnish, T., Berninger, F., Buckley, T., Farquhar, G., and Hari, P.: Challenges and Opportunities of the Optimality Approach in Plant Ecology, Silva Fennica, 36, https://doi.org/10.14214/sf.528, 2002.

https://doi.org/10.5194/egusphere-2026-3250
Preprint. Discussion started: 30 July 2026

Malek-Madani, G., Walter-Shea, E. A., Nguy-Robertson, A. L., Suyker, A., and Arkebauer, T. J.: Modeling Gross Primary Production of Midwestern US Maize and Soybean Croplands with Satellite and Gridded Weather Data, Remote Sensing, 12, 3956, https://doi.org/10.3390/rs12233956, 2020.

McColl, K. A. and Rigden, A. J.: Emergent Simplicity of Continental Evapotranspiration, Geophysical Research Letters, 47, e2020GL087 101, https://doi.org/10.1029/2020GL087101, 2020.

McColl, K. A., Wang, W., Peng, B., Akbar, R., Short Gianotti, D. J., Lu, H., Pan, M., and Entekhabi, D.: Global Characterization of Surface Soil Moisture Drydowns, Geophysical Research Letters, 44, 3682–3690, https://doi.org/10.1002/2017GL072819, 2017.

McConnaughay, K. D. M. and Coleman, J. S.: Biomass Allocation in Plants: Ontogeny or Optimality? A Test Along Three Resource Gradients, Ecology, 80, 2581–2593, https://doi.org/10.1890/0012-9658(1999)080[2581:BAIPOO]2.0.CO;2, 1999.

Miralles, D. G., Gash, J. H., Holmes, T. R. H., de Jeu, R. A. M., and Dolman, A. J.: Global Canopy Interception from Satellite Observations, Journal of Geophysical Research: Atmospheres, 115, https://doi.org/10.1029/2009JD013530, 2010.

Myneni, R., Knyazikhin, Y., and Park, T.: MOD15A2H MODIS/Terra Leaf Area Index/FPAR 8-Day L4 Global 500m SIN Grid V006, https://doi.org/10.5067/MODIS/MOD15A2H.006, 2021.

Novick, K. A., Biederman, J. A., Desai, A. R., Litvak, M. E., Moore, D. J. P., Scott, R. L., and Torn, M. S.: The AmeriFlux Network: A Coalition of the Willing, Agricultural and Forest Meteorology, 249, 444–456, https://doi.org/10.1016/j.agrformet.2017.10.009, 2018.

Noy-Meir, I.: Desert Ecosystems: Environment and Producers, Annual Review of Ecology and Systematics, 4, 25–51, https://doi.org/10.1146/annurev.es.04.110173.000325, 1973.

Paruelo, J. M., Lauenroth, W. K., Burke, I. C., and Sala, O. E.: Grassland Precipitation-Use Efficiency Varies Across a Resource Gradient, Ecosystems, 2, 64–68, https://doi.org/10.1007/s100219900058, 1999.

Pastorello, G., Trotta, C., Canfora, E., Chu, H., Christianson, D., Cheah, Y.-W., Poindexter, C., Chen, J., Elbashandy, A., Humphrey, M., Isaac, P., Polidori, D., Reichstein, M., Ribeca, A., van Ingen, C., Vuichard, N., Zhang, L., Amiro, B., Ammann, C., Arain, M. A., Ardö, J., Arkebauer, T., Arndt, S. K., Arriga, N., Aubinet, M., Aurela, M., Baldocchi, D., Barr, A., Beamesderfer, E., Marchesini, L. B., Bergeron, O., Beringer, J., Bernhofer, C., Berveiller, D., Billesbach, D., Black, T. A., Blanken, P. D., Bohrer, G., Boike, J., Bolstad, P. V., Bonal, D., Bonnefond, J.-M., Bowling, D. R., Bracho, R., Brodeur, J., Brümmer, C., Buchmann, N., Burban, B., Burns, S. P., Buysse, P., Cale, P., Cavagna, M., Cellier, P., Chen, S., Chini, I., Christensen, T. R., Cleverly, J., Collalti, A., Consalvo, C., Cook, B. D., Cook, D., Coursolle, C., Cremonese, E., Curtis, P. S., D'Andrea, E., da Rocha, H., Dai, X., Davis, K. J., Cinti, B. D., de Grandcourt, A., Ligne, A. D., De Oliveira, R. C., Delpierre, N., Desai, A. R., Di Bella, C. M., di Tommasi, P., Dolman, H., Domingo, F., Dong, G., Dore, S., Duce, P., Dufrêne, E., Dunn, A., Dušek, J., Eamus, D., Eichelmann, U., ElKhidir, H. A. M., Eugster, W., Ewenz, C. M., Ewers, B., Famulari, D., Fares, S., Feigenwinter, I., Feitz, A., Fensholt, R., Filippa, G., Fischer, M., Frank, J., Galvagno, M., Gharun, M., Gianelle, D., Gielen, B., Gioli, B., Gitelson, A., Goded, I., Goeckede, M., Goldstein, A. H., Gough, C. M., Goulden, M. L., Graf, A., Griebel, A., Gruening, C., Grünwald, T., Hammerle, A., Han, S., Han, X., Hansen, B. U., Hanson, C., Hatakka, J., He, Y., Hehn, M., Heinesch, B., Hinko-Najera, N., Hörtnagl, L., Hutley, L., Ibrom, A., Ikawa, H., Jackowicz-Korczynski, M., Janouš, D., Jans, W., Jassal, R., Jiang, S., Kato, T., Khomik, M., Klatt, J., Knohl, A., Knox, S., Kobayashi, H., Koerber, G., Kolle, O., Kosugi, Y., Kotani, A., Kowalski, A., Kruijt, B., Kurbatova, J., Kutsch, W. L., Kwon, H., Launiainen, S., Laurila, T., Law, B., Leuning, R., Li, Y., Liddell, M., Limousin, J.-M., Lion, M., Liska, A. J., Lohila, A., López-Ballesteros, A., López-Blanco, E., Loubet, B., Loustau, D., Lucas-Moffat, A., Lüers, J., Ma, S., Macfarlane, C., Magliulo, V., Maier, R., Mammarella, I., Manca, G., Marcolla, B., Margolis, H. A., Marras, S., Massman, W., Mastepanov, M., Matamala, R., Matthes, J. H., Mazzenga, F., McCaughey, H., McHugh, I., McMillan, A. M. S., Merbold, L., Meyer, W., Meyers, T., Miller, S. D., Minerbi, S., Moderow, U., Monson, R. K., Montagnani, L., Moore, C. E., Moors, E., Moreaux, V., Moureaux, C., Munger, J. W., Nakai, T., Neirynck, J.,

https://doi.org/10.5194/egusphere-2026-3250
Preprint. Discussion started: 30 July 2026

Nesic, Z., Nicolini, G., Noormets, A., Northwood, M., Nosetto, M., Nouvellon, Y., Novick, K., Oechel, W., Olesen, J. E., Ourcival, J.-M., Papuga, S. A., Parmentier, F.-J., Paul-Limoges, E., Pavelka, M., Peichl, M., Pendall, E., Phillips, R. P., Pilegaard, K., Pirk, N., Posse, G., Powell, T., Prasse, H., Prober, S. M., Rambal, S., Rannik, Ü., Raz-Yaseef, N., Rebmann, C., Reed, D., de Dios, V. R., Restrepo-Coupe, N., Reverter, B. R., Roland, M., Sabbatini, S., Sachs, T., Saleska, S. R., Sánchez-Cañete, E. P., Sanchez-Mejia, Z. M., Schmid, H. P., Schmidt, M., Schneider, K., Schrader, F., Schroder, I., Scott, R. L., Sedlák, P., Serrano-Ortíz, P., Shao, C., Shi, P., Shironya, I., Siebicke, L., Šigut, L., Silberstein, R., Sirca, C., Spano, D., Steinbrecher, R., Stevens, R. M., Sturtevant, C., Suyker, A., Tagesson, T., Takanashi, S., Tang, Y., Tapper, N., Thom, J., Tomassucci, M., Tuovinen, J.-P., Urbanski, S., Valentini, R., van der Molen, M., van Gorsel, E., van Huissteden, K., Varlagin, A., Verfaillie, J., Vesala, T., Vincke, C., Vitale, D., Vygodskaya, N., Walker, J. P., Walter-Shea, E., Wang, H., Weber, R., Westermann, S., Wille, C., Wofsy, S., Wohlfahrt, G., Wolf, S., Woodgate, W., Li, Y., Zampedri, R., Zhang, J., Zhou, G., Zona, D., Agarwal, D., Biraud, S., Torn, M., and Papale, D.: The FLUXNET2015 Dataset and the ONEFlux Processing Pipeline for Eddy Covariance Data, Scientific Data, 7, 225, https://doi.org/10.1038/s41597-020-0534-3, 2020.

Piao, S., Wang, X., Park, T., Chen, C., Lian, X., He, Y., Bjerke, J. W., Chen, A., Ciais, P., Tømmervik, H., Nemani, R. R., and Myneni, R. B.: Characteristics, Drivers and Feedbacks of Global Greening, Nature Reviews Earth & Environment, 1, 14–27, https://doi.org/10.1038/s43017-019-0001-x, 2020.

Poulter, B., Frank, D., Ciais, P., Myneni, R. B., Andela, N., Bi, J., Broquet, G., Canadell, J. G., Chevallier, F., Liu, Y. Y., Running, S. W., Sitch, S., and van der Werf, G. R.: Contribution of Semi-Arid Ecosystems to Interannual Variability of the Global Carbon Cycle, Nature, 509, 600–603, https://doi.org/10.1038/nature13376, 2014.

Prentice, I. C., Dong, N., Gleason, S. M., Maire, V., and Wright, I. J.: Balancing the Costs of Carbon Gain and Water Transport: Testing a New Theoretical Framework for Plant Functional Ecology, Ecology Letters, 17, 82–91, https://doi.org/10.1111/ele.12211, 2014.

Prentice, I. C., Balzarolo, M., Bloomfield, K. J., Chen, J. M., Dechant, B., Ghent, D., Janssens, I. A., Luo, X., Morfopoulos, C., Ryu, Y., Vicca, S., and van Hoolst, R.: Principles for Satellite Monitoring of Vegetation Carbon Uptake, Nature Reviews Earth & Environment, 5, 818–832, https://doi.org/10.1038/s43017-024-00601-6, 2024.

Reich, E., Guo, J., Peltier, D., Palmquist, E., Samuels-Crow, K., Boone, R., and Ogle, K.: Precipitation Pulse Dynamics Are Not Ubiquitous: A Global Meta-Analysis of Plant and Ecosystem Carbon- and Water-Related Pulse Responses, Global Change Biology, 31, e70 327, https://doi.org/10.1111/gcb.70327, 2025.

Reynolds, J. F. and Chen, J.: Modelling Whole-Plant Allocation in Relation to Carbon and Nitrogen Supply: Coordination versus Optimization: Opinion, Plant and Soil, 185, 65–74, https://doi.org/10.1007/BF02257565, 1996.

Reynolds, J. F., Kemp, P. R., Ogle, K., and Fernández, R. J.: Modifying the 'Pulse–Reserve' Paradigm for Deserts of North America: Precipitation Pulses, Soil Water, and Plant Responses, Oecologia, 141, 194–210, https://doi.org/10.1007/s00442-004-1524-4, 2004.

Rigden, A. J. and Salvucci, G. D.: Evapotranspiration Based on Equilibrated Relative Humidity (ETRHEQ): Evaluation over the Continental U.S., Water Resources Research, 51, 2951–2973, https://doi.org/10.1002/2014WR016072, 2015.

Robinson, D.: OPT-ing out: Root-shoot Dynamics Are Caused by Local Resource Capture and Biomass Allocation, Not Optimal Partitioning, Plant, Cell & Environment, 46, 3023–3039, https://doi.org/10.1111/pce.14470, 2023.

Rothfuss, Y., Biron, P., Braud, I., Canale, L., Durand, J.-L., Gaudet, J.-P., Richard, P., Vauclin, M., and Bariac, T.: Partitioning evapotranspiration fluxes into soil evaporation and plant transpiration using water stable isotopes under controlled conditions, Hydrological Processes, 24, 3177–3194, https://doi.org/10.1002/hyp.7743, 2010.

https://doi.org/10.5194/egusphere-2026-3250
Preprint. Discussion started: 30 July 2026

Ruehr, S., Keenan, T. F., Williams, C., Zhou, Y., Lu, X., Bastos, A., Canadell, J. G., Prentice, I. C., Sitch, S., and Terrer, C.: Evidence and Attribution of the Enhanced Land Carbon Sink, Nature Reviews Earth & Environment, 4, 518–534, https://doi.org/10.1038/s43017-023-00456-3, 2023.

Sala, O. E., Parton, W. J., Joyce, L. A., and Lauenroth, W. K.: Primary Production of the Central Grassland Region of the United States, Ecology, 69, 40–45, https://doi.org/10.2307/1943158, 1988.

Schymanski, S. J., Or, D., and Zwieniecki, M.: Stomatal Control and Leaf Thermal and Hydraulic Capacitances under Rapid Environmental Fluctuations, PLOS ONE, 8, e54 231, https://doi.org/10.1371/journal.pone.0054231, 2013.

Seneviratne, S. I., Corti, T., Davin, E. L., Hirschi, M., Jaeger, E. B., Lehner, I., Orlowsky, B., and Teuling, A. J.: Investigating Soil Moisture–Climate Interactions in a Changing Climate: A Review, Earth-Science Reviews, 99, 125–161, https://doi.org/10.1016/j.earscirev.2010.02.004, 2010.

Short Gianotti, D.: Monotone Copula Filter, Zenodo, https://doi.org/10.5281/zenodo.17460263, 2025.

Short Gianotti, D. J. and Entekhabi, D.: Local and General Patterns of Terrestrial Water-Carbon Coupling, Geophysical Research Letters, 51, e2024GL109 625, https://doi.org/10.1029/2024GL109625, 2024.

Short Gianotti, D. J., Rigden, A. J., Salvucci, G. D., and Entekhabi, D.: Satellite and Station Observations Demonstrate Water Availability's Effect on Continental-Scale Evaporative and Photosynthetic Land Surface Dynamics, Water Resources Research, 55, 540–554, https://doi.org/10.1029/2018WR023726, 2019.

Short Gianotti, D. J., McColl, K. A., Feldman, A. F., Xu, X., and Entekhabi, D.: Two Sub-Annual Timescales and Coupling Modes for Terrestrial Water and Carbon Cycles, Global Change Biology, 30, e17 463, https://doi.org/10.1111/gcb.17463, 2024.

Stocker, B. D., Zscheischler, J., Keenan, T. F., Prentice, I. C., Peñuelas, J., and Seneviratne, S. I.: Quantifying Soil Moisture Impacts on Light Use Efficiency across Biomes, New Phytologist, 218, 1430–1449, https://doi.org/10.1111/nph.15123, 2018.

Stoy, P. C., El-Madany, T. S., Fisher, J. B., Gentine, P., Gerken, T., Good, S. P., Klosterhalfen, A., Liu, S., Miralles, D. G., Perez-Priego, O., Rigden, A. J., Skaggs, T. H., Wohlfahrt, G., Anderson, R. G., Coenders-Gerrits, A. M. J., Jung, M., Maes, W. H., Mammarella, I., Mauder, M., Migliavacca, M., Nelson, J. A., Poyatos, R., Reichstein, M., Scott, R. L., and Wolf, S.: Reviews and Syntheses: Turning the Challenges of Partitioning Ecosystem Evaporation and Transpiration into Opportunities, Biogeosciences, 16, 3747–3775, https://doi.org/10.5194/bg-16-3747-2019, 2019.

Swann, A. L., Fung, I. Y., and Chiang, J. C.: Mid-Latitude Afforestation Shifts General Circulation and Tropical Precipitation, Proceedings of the National Academy of Sciences of the United States of America, 109, 712–716, https://doi.org/10.1073/pnas.1116706108, 2012.

Trugman, A. T., Medvigy, D., Mankin, J. S., and Anderegg, W. R. L.: Soil Moisture Stress as a Major Driver of Carbon Cycle Uncertainty, Geophysical Research Letters, 45, 6495–6503, https://doi.org/10.1029/2018GL078131, 2018.

Walter, H.: Grassland, Savanne Und Busch Der Arideren Teile Afrikas in Ihrer Ökologischen Bedingtheit, Jahresbericht über die Fortschritte der wissenschaftlichen Botanik, 87, 750–860, 1939.

Wang, H., Bassiouni, M., Kang, Y., Rifai, S. W., Gherardi, L. A., Ukkola, A., and Keenan, T. F.: Soil Moisture Buffers the Impact of Precipitation Variability on Ecosystem Productivity, Water Resources Research, 62, e2025WR041 521, https://doi.org/10.1029/2025WR041521, 2026.

Wheeler, K. I. and Dietze, M. C.: A Trigger May Not Be Necessary to Cause Senescence in Deciduous Broadleaf Forests, bioRxiv, p. 2023.06.07.544057, https://doi.org/10.1101/2023.06.07.544057, 2023.

Wilcox, K. R., Shi, Z., Gherardi, L. A., Lemoine, N. P., Koerner, S. E., Hoover, D. L., Bork, E., Byrne, K. M., Cahill Jr., J., Collins, S. L., Evans, S., Gilgen, A. K., Holub, P., Jiang, L., Knapp, A. K., LeCain, D., Liang, J., Garcia-Palacios, P., Peñuelas, J., Pock-

https://doi.org/10.5194/egusphere-2026-3250
Preprint. Discussion started: 30 July 2026

man, W. T., Smith, M. D., Sun, S., White, S. R., Yahdjian, L., Zhu, K., and Luo, Y.: Asymmetric Responses of Primary Productivity to Precipitation Extremes: A Synthesis of Grassland Precipitation Manipulation Experiments, Global Change Biology, 23, 4376–4385, https://doi.org/10.1111/gcb.13706, 2017.

Williams, C. A. and Albertson, J. D.: Contrasting Short- and Long-Timescale Effects of Vegetation Dynamics on Water and Carbon Fluxes in Water-Limited Ecosystems, Water Resources Research, 41, https://doi.org/10.1029/2004WR003750, 2005.

Wright, I. J., Reich, P. B., and Westoby, M.: Least-Cost Input Mixtures of Water and Nitrogen for Photosynthesis., The American Naturalist, 161, 98–111, https://doi.org/10.1086/344920, 2003.

Xiao, Z., Wang, T., Liang, S., and Sun, R.: Estimating the Fractional Vegetation Cover from GLASS Leaf Area Index Product, Remote Sensing, 8, 337, https://doi.org/10.3390/rs8040337, 2016.

Yang, Y., Roderick, M. L., Guo, H., Miralles, D. G., Zhang, L., Fatichi, S., Luo, X., Zhang, Y., McVicar, T. R., Tu, Z., Keenan, T. F., Fisher, J. B., Gan, R., Zhang, X., Piao, S., Zhang, B., and Yang, D.: Evapotranspiration on a Greening Earth, Nature Reviews Earth & Environment, 4, 626–641, https://doi.org/10.1038/s43017-023-00464-3, 2023.

Zeng, Y., Hao, D., Park, T., Zhu, P., Huete, A., Myneni, R., Knyazikhin, Y., Qi, J., Nemani, R. R., Li, F., Huang, J., Gao, Y., Li, B., Ji, F., Köhler, P., Frankenberg, C., Berry, J. A., and Chen, M.: Structural Complexity Biases Vegetation Greenness Measures, Nature Ecology & Evolution, 7, 1790–1798, https://doi.org/10.1038/s41559-023-02187-6, 2023.

Zeng, Z., Piao, S., Li, L. Z. X., Wang, T., Ciais, P., Lian, X., Yang, Y., Mao, J., Shi, X., and Myneni, R. B.: Impact of Earth Greening on the Terrestrial Water Cycle, Journal of Climate, 31, 2633–2650, https://doi.org/10.1175/JCLI-D-17-0236.1, 2018.

Zhao, M., A, G., Liu, Y., and Konings, A. G.: Evapotranspiration Frequently Increases during Droughts, Nature Climate Change 2022 12:11, 12, 1024–1030, https://doi.org/10.1038/s41558-022-01505-3, 2022.

Zhu, P., Zhuang, Q., Ciais, P., Welp, L., Li, W., and Xin, Q.: Elevated Atmospheric CO2 Negatively Impacts Photosynthesis through Radiative Forcing and Physiology-Mediated Climate Feedback, Geophysical Research Letters, 44, 1956–1963, https://doi.org/10.1002/2016GL071733, 2017.